RECENT EXPERIMENTS IN HYPERSONIC TURBULENT BOUNDARY LAYERS

By Mitchel H. Bertram and Luther Neal, Jr.

NASA Langley Research Center
Langley Station, Hampton, Va., U.S.A.

Presented at the AGARD Specialists Meeting
on Recent Developments in Boundary-Layer Research
Sponsored by the Fluid Dynamics Panel of AGARD

Naples, Italy
May 10-14, 1965

NATIONAL AERONAUTICS AND
SPACE ADMINISTRATION
WASHINGTON

RECENT EXPERIMENTS IN HYPERSONIC TURBULENT BOUNDARY LAYERS

By Mitchel H. Bertram[1] and Luther Neal, Jr.[2]

NASA Langley Research Center

ABSTRACT

22565

Considering the numerous and often differing theories available for determining the behavior of compressible turbulent boundary layers a choice of prediction method is often determined by the available experimental data. This paper considers this problem in the light of the results of recent experiments in a number of different facilities and from flight. The data for skin friction and heat transfer are generally from sharp flat plate and pointed cone models and are now available for very cold walls up to Mach numbers of approximately 9. Mach number and wall-temperature effects from these experiments are compared to the more recent prediction methods. In addition, an evaluation of the maximum heat transfer and shear stress to be encountered on smooth flat plates and cones is made. Since boundary-layer structure is an important consideration, boundary-layer velocity and temperature profiles obtained on hollow cylinders and nozzle walls are considered.

INTRODUCTION

A large number of methods for predicting the behavior of compressible turbulent boundary layers have accumulated over the years. Often the results from these methods differ widely and recourse to experiments must be made. In turn the methods themselves are often based on experiments so that an alternating procedure develops. In our case, we will bring to bear on this problem the results of recent experiments in a number of different facilities and from various organizations.[3]

The results for heat transfer and skin friction that are presented here are in general restricted to the flat plate with a "sharp" leading edge and the pointed cone; however, boundary-layer profiles obtained on hollow cylinders and nozzle walls are also presented. Evaluating the data obtained on the flat plate and cone models is complicated by problems such as establishing the

---

[1]Head, Hypersonic Branch.

[2]Aerospace Engineer.

[3]The authors' wish to acknowledge the invaluable aid from researchers in a number of organizations who provided a great deal of the unpublished data contained in this paper. Particularly to be noted is the cooperation of the Gasdynamics Branch of the Air Force Flight Dynamics Laboratory at Wright-Patterson Air Force Base, Ohio and of the McDonnell Aircraft Corporation and the Republic Aviation Corporation. Their contributions and those of NASA Langley Research Center and Flight Research Center personnel are specifically noted at the appropriate places in this paper.

virtual origin of the boundary layer, the Reynolds analogy factor, and the relationship of results obtained on cones to those obtained on flat plates; these problems are discussed in the presentation.

The results allow a simultaneous assessment of wall-temperature effect and Mach number effect (Mach numbers up to about 9) in relation to the more recent prediction methods. Additionally, consideration is given to evaluating the maximum heat transfer and skin friction that is encountered on smooth flat plates and cones from very low to hypersonic speeds.

SYMBOLS

a.w.	adiabatic wall
C_F	average skin-friction coefficient
C_f	local skin-friction coefficient
$C_{f,i,x}$	incompressible value of turbulent C_f at value of $R_{l,x}$ where peak in C_f occurs $(R_{l,p})$
d	leading-edge thickness
f.p.	flat plate
h	enthalpy
L(K)	Karman mixing length
L(P)	Prandtl mixing length
M	Mach number
n	inverse of the exponent in the power law for skin friction
N_{Pr}	Prandtl number
N_{St}	heat-transfer coefficient (Stanton number)
$N_{St,c}$	heat-transfer coefficient with boundary-layer turbulent from cone apex
$N_{St,i,c}$	incompressible value of Stanton number at $R_v/2$
$N_{St,i,x}$	incompressible value of Stanton number at value of $R_{l,x}$ where peak in N_{St} occurs $(R_{l,p})$
r	radius of axisymmetric nozzle

R	Reynolds number
R_θ	Reynolds number based on momentum thickness
R_v	Reynolds number based on local conditions and distance from peak shear or peak heating
$R_{l,p}$	value of $R_{l,x}$ where peak shear or peak heating occurs
$R_{l,x}$	Reynolds number based on local conditions and distance from leading edge
t	time
T	temperature
u	local velocity in boundary layer
U	velocity outside boundary layer
y	distance measured from surface, normal to surface
α	angle of attack
δ^*	displacement thickness of boundary layer
θ	momentum thickness of boundary layer
θ_c	semiapex angle of cone
ω	exponent in power law for viscosity

Subscripts:

aw	adiabatic wall
c	cone
fp	flat plate
i	incompressible value
l	local value
p	peak value
t	total value
tc	truncated cone

w	wall
∞	free stream

DATA ANALYSIS

Of importance in evaluating sets of data which cover a large range of conditions is the determination of a virtual origin, which is hopefully consistent. Among many assumptions one can use (a) the physical leading edge; (b) the start of transition [1]; (c) the end of transition (say, the place of peak shear stress or peak heating) [2] [3] [4]; or (d) match the momentum loss across an abrupt transition point and theoretically determine a hypothetical start for the turbulent boundary layer [5] [6].

The first three assumptions were checked against a large body of heat-transfer data obtained at the Langley laboratory and certain low speed experiments. The only one of these various assumptions of effective boundary-layer origin, which was reasonably consistent for the bulk of the data was assumption (c) which utilizes the peak shear stress or peak heating as the origin, thus agreeing with Coles early work [2]. This assumption of virtual origin was used for the work reported in this paper. As a consequence of using this virtual origin, only data where a peak can be identified, or where transition close to a trip device occurs, can be used. Assumption (d) or momentum matching is most attractive from the standpoint of being the least arbitrary but requires a priori selection of a compressible theory for its utilization in general.

Low speed heat-transfer data [6] are shown in figure 1 with Reynolds numbers based on distance from the leading edge and from the assumed virtual origin (peak). In the turbulent case the Kármán-Schoenherr equation for local skin-friction coefficient modified by the analogy between heat transfer and momentum according to von Kármán is shown for comparison purposes. (See appendix A for the incompressible formulas used.) The data generally show good agreement with the theory when measured from the peak location. Exceptions are the data at the lowest Reynolds numbers (i.e., closest to the peak) and the data where natural transition occurred. This result at the lowest Reynolds numbers is expected considering the shape of the experimental curve. However, the difficulty with the natural transition data is believed due to the use of the indicated peak in the data which form a long shallow curve in the region of the peak. A relatively small forward correction to the peak location would put these data in good agreement with the other data and the theory.

It might be well to point out here that the Reynolds analogy factor chosen to modify the skin-friction equation can have a significant influence on the level of the experimental data in the form of the $N_{St}/N_{St,i}$ ratio. The Kármán analogy factor used [7] (with $N_{Pr} = 0.725$, for this paper) is within ± 2 to ± 3 percent of that given by the more recent papers of Deissler-Loeffler

(M = 0) [8] and Tetervin [9] but is 9 to 11 percent lower than the value given by the Colburn analogy ($N_{Pr}^{-2/3}$ with $N_{Pr} = 0.725$) for $10^6 < R_v < 10^7$ and there are still greater differences at higher Reynolds numbers.

Examples of some high-speed unmodified data are shown in figure 2(a). These data were obtained by Cary in the Langley 20-inch hypersonic tunnel on a flat plate 16 inches long and 11 inches in span. Data at three pressure levels and two angles of attack are shown. The highest angle of attack reduces the free-stream Mach number of 6 to a local Mach number of 4. The known effect of leading-edge thickness and unit Reynolds number on boundary-layer transition [10] seem sufficient to explain the movement of transition with changes in pressure level and here one may note that station A and station B designated on the figure are located one-half inch on either side of the model center line or only one inch apart. However, we are not so much concerned with transition per se as in simply knowning where the peak occurs.

These same data plus data obtained at other angles of attack are presented in figure 2(b) with Reynolds number based on distance from the peak heating value. In this case the experimental points have been divided by the values given by the modified Kármán-Schoenherr equation at the corresponding values of R_v. One can see that for R_v greater than about 10^6 the normalized heat-transfer coefficient is virtually independent of Reynolds number. The same result is indicated by data shown in figure 3 obtained in the Langley 18-inch variable density wind tunnel on the same model tested at a free-stream Mach number of 8 by Weinstein.

Both skin friction and heat transfer have been obtained on a flat plate by Neal in the Langley 11-inch hypersonic tunnel and are shown in figure 4. In this case the model was 10 inches in span and 24 inches long; however, the tunnel test core width was 5 to 6 inches. Data is shown to a distance of 19.75 inches from the leading edge along the model center line. Visual studies using surface oil flow indicated some side edge effect near the trailing edge. Skin friction was obtained by the floating element technique and the heat transfer by using thermocouples in a thin skin. Different leading edges were used for the skin friction and the heat-transfer measurements, and even though both measured about 0.001 inch thick, undetected differences between the two leading edges may explain the change in transition Reynolds number between the two sets of data. This however does not explain the insensitivity of transition to pressure level. The heating data as a function of distance from the peak heating (R_v) shows much the same behavior as the experiments presented in figures 1 to 3 although there is a tendency for this data to show a slight decrease for the highest values of R_v. This may be attributable to the side edge effects previously mentioned.

Thus far the data considered has been from flat-plate models; however, much of the data available is from cones. According to Van Driest [11] the local skin-friction coefficient on a cone is the same as that on a flat plate at half the local Reynolds number on the cone. This rule however applies only

to cones where the flow is turbulent from the apex; in the actual case transition occurs at a significant distance downstream of the apex and the turbulent boundary layer would be expected to behave more as if it were growing on a truncated cone. A transformation has been applied to the data obtained on cones to correct the results to the values that would be obtained were the flow turbulent from the apex of the cone. The details of this transformation are given in appendix B.

Two sets of data obtained on cones in supersonic wind-tunnel flow [12] [13] are shown in figure 5. Here only the data downstream of peak heating are shown. The heat-transfer coefficient has been normalized with respect to the incompressible heat-transfer coefficient, as for the data in figures 2 to 4, except that the incompressible value at half the Reynolds number (R_V) of interest is used, designated in this case $N_{St,i,c}$. For this and the remainder of the cone results, the data is reduced in terms of local values on the cone surface [14]. The amount that the original data (open symbols) lies below the modified data (filled symbols) indicates the reduction in heat-transfer coefficient that theory predicts to be due to the location of turbulent flow downstream of the cone apex. The effect is seen to be significant.

The results of three separate flight experiments [15] [16] [17] are given in figure 6. One notes that the original normalized heating coefficient data values (fig. 6(a)) are generally increasing with increasing Reynolds number (R_V). This sort of effect is predicted by the theory taking the "turbulent cone truncation" into account. (One can note a general tendency of this type in the overall original data of figure 5, but the restricted range of R_V and data scatter did not allow definite conclusions to be drawn.) Upon examining the individual series of datum points corrected to turbulent flow from the apex (fig. 6(b)), the effect of Reynolds number on the Stanton number ratio is, at least, found to be significantly reduced. (Datum points close to the place where peak heating occurs are not included in the corrected data; these may readily be identified by comparing the two parts of figure 6 in the lower range of R_V.)

Of considerable value is the hitherto unpublished data, from cone models, contained in figure 7. These data cover a considerable range of wall temperature ratio and most importantly extend down to very low wall temperature ratios. The upper set in figure 7(a) is derived from data supplied by the Republic Aviation Corporation from tests in their 36-inch-diameter pebble bed heated, closed jet, hypersonic wind tunnel.[4] The lower set is an adaption of data supplied by the McDonnell Aircraft Corporation from tests that were run in the Cornell Aeronautical Laboratory 48-inch hypersonic shock tunnel.[5] The manner in which wall-temperature ratio was varied was different for these two sets of data. For the Republic data the supply temperature was kept roughly constant and the wall temperature was varied by cooling or heating the model. In the case of the McDonnell data, the wall temperature was always about room temperature and the wall-temperature ratio was varied by using a number of different

[4]U.S. Air Force contract AF 33(657)-9697.
[5]U.S. Air Force contract AF 04(694)-390.

supply enthalpies. Again the correction for "turbulent cone truncation" reduces the effect of Reynolds number on the Stanton number ratio (fig. 7(b)); though the effect of Reynolds number in the case of the Republic data is more than would be expected, it is not considered excessive.

EFFECT OF WALL-TEMPERATURE RATIO ON HEAT TRANSFER

In the previous section the data was considered from the standpoint of its proper reduction and interpretation rather than examining trends or evaluating predictions. Here we will examine the data in relation to the prediction methods. One of the important points to be resolved in the turbulent boundary-layer problem is the effect of wall-temperature ratio on the heat-transfer (or skin-friction) ratio. To investigate this problem in some detail, figures 8, 9, and 10 have been prepared to cover the supersonic-hypersonic range and to compare flight and wind-tunnel results where possible.

Data obtained in the supersonic range between Mach numbers of 3 and 4 are shown in figure 8. These data are average values of the data contained in figures 2(b), 5, 6(b), and [18]. The measurements contained in [18] were taken on the cylindrical portion of a cone cylinder. The actual Mach numbers shown are 3.3 and 3.8. Where the Mach number of the test was different from these Mach numbers, the predicted incremental effect of Mach number on the heating coefficient ratio was added to the datum value. In this range of Mach numbers there is an insignificant difference between the various theories in the predicted increment of skin friction or heat transfer due to a small change in Mach number. The theories shown are the much used T-prime or reference temperature method using Monaghan's constants as given in [19] and the more recent semiempirical formulation for skin friction of Spalding-Chi [20] modified to heat transfer as given in appendix A.

The trend though not the magnitude of the $M = 3.3$ data is predicted quite well by the T-prime method and the trend of the $M = 3.8$ data appears to be intermediate between the T-prime and the modified Spalding-Chi predictions.[6] At both Mach numbers there is generally good agreement between the flight and wind-tunnel results. It may be noted that the T-prime method was computed for a nominal flight temperature at both Mach numbers. Computing the T-prime result for the lowest wind-tunnel total temperature (500° R) raises the prediction about 5 percent over the curves shown. As given, the Spalding-Chi method does not include an effect of total temperature level. The $M = 3.3$ data are considerably and consistently above both prediction methods - an unexplained effect. However, data obtained on wing panels during flights of the X-15 by Banner, Kuhl, and Quinn of the NASA Flight Research Center at a Mach number of 3 do not agree with the high level indicated by the $M = 3.3$ data in figure 8. In the case of the X-15 data at a Mach number of 3, which is shown on

[6]Coles results [2] for local skin friction at $M = 3.7$ with an adiabatic wall $\left(T_w/T_t \approx 0.9\right)$ give a value for $C_f/C_{f,i}$ of about 0.54 thus fitting in quite well with the heat-transfer data.

the left-hand side of figure 9 by the shaded rectangle, there is good agreement with the modified Spalding-Chi prediction. As shown to the right in this figure, X-15 data at a Mach number of 5 still agree best with the modified Spalding-Chi prediction, but the mean of the data appears to lie somewhat below the prediction. The value of $N_{St,i}$ used to normalize the experimental heat-transfer coefficients is from the modified Kármán-Schoenherr equation as for the other data presented in this paper.

Flight data are desirable but because such data generally cannot be obtained under as well controlled conditions as are possible in wind tunnels, doubts can always remain where such experiments are our major source of information. Thus much of the available experimental results from wind tunnels have been collected in figure 10 to aid in evaluating the wall-temperature effect. The data are in the low hypersonic speed range (roughly, Mach numbers from 5 to 9) where the large temperature potential driving heat transfer aids in obtaining more accurate data than are generally obtained in the supersonic speed range in wind-tunnel flows. The results shown are average values from figures 2(b), 3, 4, and 7(b) plus additional data from [18], [21], [22], and [23].

For the data shown in figure 10 which were obtained by the conventional thin wall thermocouple or thin-film techniques (solid symbols), good agreement is found with the trend of the Spalding-Chi predictions. The T-prime method significantly overpredicts the heat transfer at the lowest wall-temperature ratios. This overprediction is not apparent unless the wall-temperature ratio is considerably below 0.5 at $M \approx 5$ and less than 0.3 to 0.4 at $M \approx 8$. The NOL and APL data [21], [22], and [23] (open symbols) generally do not agree with the other data. The Winkler-Cha formulation [21] was designed to fit the NOL data, which it does quite well, but except for Hill's data considerably underpredicts the other data including the X-15 results previously presented (fig. 9). The NOL heat-transfer results were obtained from inner wall-temperature measurements and the data of Hill were obtained from boundary-layer profiles; Winkler and Cha's results were on a flat plate, Lobb, Winkler, and Persh obtained their results in a wedge nozzle, and Hill's results were obtained in a conical nozzle utilizing nitrogen gas.

Going back to the data represented by the solid symbols in figure 10, one notes that, although the modified Spalding-Chi method best represents the data of all the theories shown, it does somewhat underpredict the data. The underprediction is generally from 5 to 15 percent with one point at Mach 8 about 25 percent underpredicted. This discrepancy appears to be a function of, and increasing with, Mach number. It is perhaps best seen in the original presentation of the data in figures 2(b), 3, 4, and 7. It is clear that we cannot at this point say that this represents a basic effect, for the problem of the proper form of the Reynolds analogy factor relating skin friction and heat transfer has not been solved. For instance, using Colburn's form of Reynolds analogy (discussed earlier) would bring the prediction into somewhat better agreement with the higher Mach number results but would result in poorer agreement for the lower Mach number data (fig. 1 results and fig. 2(b) $M = 4$). There are possible, however, other explanations for this type of behavior.

Various turbulent theories are quite plastic in their behavior depending on the assumptions which go into their makeup. The predictions of average and local skin-friction ratios on an insulated flat plate as a function of Mach number by various theories [20], [24], [25] are shown in figure 11. Previously in this paper we have avoided such a presentation of theory because of the difficulty of comparing data and theory on such a plot when, in addition to the conditions shown, the problem of the large range of wall-temperature ratios and stream conditions has to be added. Often in the past such plots on which are placed all available theories have been used as a horrible example to show the large discrepancies between theories. Here our intention is more to show the wide variations in prediction possible within a given theory.

Generally the more complete theories show an effect of stream temperature level. In this case, this is illustrated by showing calculations for two limits of the exponent in the power law for viscosity, $\omega = 0.5$, which corresponds to a high Mach number - high temperature flow, and $\omega = 1$, an arbitrary upper limit which might correspond to a very cold flow. (For the tests presented in this paper ω generally varied between 0.8 and 1.) In addition, the analytic result depends upon the law assumed for the mixing length; either the Prandtl mixing length (L(P)) or the Kármán mixing length (L(K)) are generally used. Li and Nagamatsu [25] also introduce a proportionality constant or "compressibility mixing length parameter" which determines the importance of the contribution to the shearing stress from density fluctuations. When the proportionality constant in the Li-Nagamatsu theory is zero, the result is the same as that given by the Van Driest theory [24]. Since the exponent ω is generally known, the most important determinations are that of the proper mixing length and of the contribution of the density fluctuations. The Spalding-Chi method is semiempirical and does not, as given, allow a choice of mixing length or values of ω. The T-prime method, included for reference, does not have mixing length considerations. Figure 11 was prepared for a Reynolds number of 10^7. Changing the Reynolds number by an order of magnitude, say, would change the curves shown but this would probably be a second-order effect.

In the Li-Nagamatsu paper local skin friction and heat transfer and the effect of wall-temperature ratio are not treated directly; however, because of its similarity with the Van Driest analysis together with the increase in skin friction due to the inclusion of density fluctuation terms, it is possible that an extension to this theory may give a good prediction of heating at the higher Mach numbers if the Kármán mixing length is assumed to be the proper one. This result can only be considered tentative and definitive answers will probably have to await experiments at still higher Mach numbers than have been presented here. If this result is correct, however, higher heat-transfer rates than are predicted by the Spalding-Chi method will have to be anticipated at high Mach numbers.

The effect of wall-temperature ratio was one of our major considerations in the data in figures 8 to 10. How the local skin-friction ratios presented in figure 11 for the insulated wall case are affected by temperature ratio is shown in figure 12. Again the limits for the viscosity-temperature relation

exponent are taken as 0.5 and 1 (except for the Spalding-Chi method) and where applicable both the Prandtl and Kármán mixing length results are shown. At the lower Mach number ($M = 4$) the differences between the various assumptions within a theory and between the theories is much less than at the higher Mach number. At $M = 20$ skin friction covers the gamut from increasing to decreasing with decreasing wall temperature. With one (the Van Driest) theory virtually all the possibilities can be obtained, depending upon the assumptions used in the calculations, including the case where the skin friction is practically independent of wall temperature. This latter case is similar to results from the Spalding-Chi method though the numerical values are higher (even taking into account that the value of ω used in computing the Van Driest theory in figure 12 would have to be reduced in order to more closely correspond to the ω of the data used by Spalding-Chi in formulating their result). Because of the sensitivity of this and similar theories to the various assumptions, there is more likelihood of definitive experiments being performed in the hypersonic speed range than at lower speeds.

THE MAXIMUM HEAT TRANSFER TO SMOOTH FLAT PLATES AND CONES

Up to this point the results do not allow an evaluation of the maximum heat transfer to be encountered on smooth flat plates and cones. This maximum is closely represented by the peak in heating which has been used to designate the virtual origin of the turbulent boundary layer in the previous section of this paper. Examples of the peaks shown by experimental heating distributions are contained in the upper portion of figure 1 and in figure 2(a) while in the upper portion of figure 4 such peaks are shown in both shear and heating distributions.

Figure 13 has been prepared to show the values of peak heating $\left(N_{St,p}\right)$ obtained on flat plates on both low speed [6] and high-speed flow as a function of Reynolds number based on the distance from the leading edge to the peak heating location. The high-speed data is that used to compose figures 2, 3, and 4, plus unpublished data obtained by Sterrett in the Langley 20-inch hypersonic tunnel and data contained in [26]. The values of the peak in the heat-transfer coefficient show much the same variation with Reynolds number shown by the incompressible turbulent theory (Kármán-Schoenherr). This suggests utilizing this theory to remove much of the Reynolds number dependence as is done in the lower portion of the data presentation in figure 13 for each speed range. In this form the Reynolds number dependence is indicated to be weak; however, a definite dependence on Mach number is shown.

A means for predicting these peak values would be desirable. Momentum matching, which was discussed in an early part of this paper, suggests itself. The result from momentum matching for incompressible flow using the Blasius equation for laminar skin friction, and the Kármán-Schoenherr equation for turbulent skin friction is shown in the upper part of figure 13. The agreement with the data is surprisingly good considering that the theory assumes sudden

transition and the actual transition can be a gradual process as shown in figure 1.

Application of this method to the compressible results shown in the lower part of figure 13 met with mixed results. Utilizing the Spalding-Chi formulation [20] with the Blasius equation modified to compressible flow by the T-prime method gave good agreement with $M_l = 4$ results but underpredicted the data by increasing amounts as the Mach number increased until at $M_l = 8$ it was about 35 percent below the data. Some rough calculations with Li-Nagamatsu theory [25] for the turbulent flow gave values within 10 percent of the $M_l = 8$ data. These calculations are not shown, as at present they require too much judgment for application (only the curves of figure 11 were available, limited to a Reynolds number of 10^7, adiabatic wall, and average skin friction).

Another way of looking at peak data is to compare it with data downstream of the assumed virtual origin, which was shown previously to have a similar trend with Mach number. Figure 14 presents these results in the form of the peak heating (or skin-friction) ratio divided by the heating (or skin-friction) ratio downstream of the virtual origin. The data is generally from sources cited earlier in this paper where the test conditions are given in some detail with the addition of Coles skin-friction data [2] taken under adiabatic wall and essentially room temperature supply conditions. To avoid a confusion of symbols, only average values are shown for the large number of peak results available from a given source.

The flat-plate results for this ratio on figure 14 while not conclusive appears to be independent of Mach number and the level agrees with that found for incompressible flow by the momentum matching procedure. For all the flat-plate data except the low-speed results the values of $R_{l,p}$ and R_v are of the same magnitude. (The low-speed data were compared to results of momentum matching for the proper Reynolds number in figure 13.)

The same ratio from cone data is about 20 percent below the flat-plate results and appears also to be essentially independent of Mach number. (Note that the flight results are for Reynolds numbers about one order of magnitude higher than the other flat-plate or cone results shown.) Based on these results the prediction of the entire heat-transfer (or skin-friction) behavior on a flat plate or cone depends upon the ability to predict the $N_{St}/N_{St,i}$ (or $C_f/C_{f,i}$) ratio.

BOUNDARY-LAYER SURVEYS

In the previous discussion, only gross effects of the turbulent boundary layers have been considered, i.e., skin friction and heat transfer. However, it is clear that a general understanding of the mechanisms at work within the boundary layer itself is needed for fully evaluating turbulent data and theories.

Some of the basic structure of the boundary layer can be obtained from conventional boundary-layer pressure and temperature surveys; however, because of the relative thinness of the laminar sublayer as compared to the overall boundary-layer thickness, small probes or thick boundary layers, or both, are necessary for probing in this region.

Figure 15 is composed of recently obtained velocity and temperature profiles in relatively thick boundary layers (2 to 4 in.) at Mach numbers of 6 and 6.8 in air and 18.5 in helium. The ratios of wall to free-stream stagnation temperature are 0.63, 0.50, and 1, respectively. This data was obtained on nozzle walls near the test section where the longitudinal pressure gradients were, for all practical purposes, zero. The Mach 6.0 data were obtained by Cary in the Langley 20-inch hypersonic tunnel, the Mach 6.8 data were obtained by Neal in the Langley 11-inch hypersonic tunnel, and the Mach 18.5 data were obtained by Watson in the Langley 22-inch helium tunnel.[7] The velocity profiles were obtained from local pitot pressure measurements and faired values of local stagnation temperature measurements[8] in conjunction with the conventional assumption of constant static pressure through the boundary layer. A recovery factor of unity was used for the temperature probes as time did not permit a comprehensive calibration of the probes; however, calibration of probes identical to those used to gather the data, at Mach numbers of 6.0, 6.8, and 8.5, over a sizable range of unit Reynolds numbers gave recovery factors of unity. The recovery factor for these probes may or may not be unity at flow conditions encountered well within the boundary layer and especially near the wall.

General examination of the velocity profiles in figure 15 show that they display the typical appearance of turbulent boundary layers, i.e., an outer region that can be represented quite well with a power law, an inner region, or laminar sublayer, and of course the intermediate, or buffer, region between the two. Closer examination of the profiles show that at a given Mach number the inverse of the exponent in the power law fit to the outer region increases with R_θ, that there is a small inflection point near the edge of the boundary layer, that the laminar sublayer thickness (which is very small for the air data) increases with decreased Reynolds number, and that the values of C_f deducible from the velocity profiles could not be called conclusive. Walz [27] has criticized the validity of the C_f data of references [21] and [22] as well as Hill's older results [28] which were obtained from velocity profiles. Figure 16 is composed of portions of representative velocity profiles from references [21] and [22] at a Mach number near 5. Included in these plots are results from reversed calculations using the values of C_f (and other pertinent quantities) given in the references and using the viscosity law given by equation (A1). In

[7]Note on figure 15(c) that the boundary-layer thickness covers about half the radius of the nozzle, and thus significant lateral curvature effects are probably present.

[8]In general, the wall-distances at which the temperature measurements were made differed from those where the pressure measurements were made so faired values of the temperature data were used in computing the velocity profiles.

several instances, and especially at the lower values of $T_w/T_{t,\infty}$ it is difficult to determine how conclusive values of C_f could be deduced. The dashed curves, which were inversely computed from Spalding and Chi's [20] theoretical C_f values are shown here, and elsewhere on all the velocity profiles, except the one in helium, as reference lines. In many cases there is good agreement of experiment with the Spalding-Chi predictions; in others it is difficult to determine whether the disagreement is a fundamental one or a result of probe inaccuracies and interference effects near the wall.

Returning to figure 15 for the temperature profiles, it is seen that $T_t/T_{t,\infty}$ versus log y is roughly linear for the air data with some dependence on R_θ. The single profile taken in helium has a bowl-like shape, the lower value $\left(T_t/T_{t,\infty} \approx 0.92\right)$ is probably close to the value that would be obtained at an insulated wall. There is some scatter in the $M = 6.8$ temperature profiles which is believed due to changes with time in the previous history of the flow. During the gathering of this data it was observed that for a given y location, the measured values of $T_t/T_{t,\infty}$ gradually increased with time (available run time approximately 60 seconds). This probably resulted from sizable increases with time in the temperature of the nozzle wall upstream of the probing region. The test-section region, which is massive in structure and has relatively low heating rates, did not significantly increase in temperature during a run. Therefore, only temperature data taken near the start of the run (approximately 10 seconds) has been used since this data would correspond more nearly to a uniform wall temperature close to that measured in the probing region. The Mach 6.0 profiles, which were taken in a slow starting but long running time capability tunnel, and the Mach 18.5 profile, which was taken in a facility operating with a stagnation temperature near ambient temperature, were not found to be time dependent.

Velocity and temperature profiles recently obtained by Adcock and Peterson on a hollow cylinder model in the Mach 6.0 Langley 20-inch hypersonic tunnel at $T_w/T_{t,\infty}$ values of 0.38, 0.49, and 0.89 are shown in figure 17. Qualitatively, the data for the nonadiabatic wall temperature cases, agrees with the Mach 6.0 nozzle wall data previously presented in figure 15(a) except for the overshoot in $T_t/T_{t,\infty}$. An overshoot in $T_t/T_{t,\infty}$ for the adiabatic wall case is to be expected in order to conserve energy;[9] however, this data shows a higher degree of overshoot for the nonadiabatic wall temperature cases than for the adiabatic one. Experimental difficulties with the small probes used to sursurvey the relatively thin boundary layers on the hollow cylinder possibly account for this behavior. By interpolating this hollow cylinder data for a $T_w/T_{t,\infty} \approx 0.63$ and extrapolating the nozzle wall data of figure 15(a) to lower values of R_θ, it is seen that the resulting power in the power law fit to the outer u/U profiles do not agree. This result suggests that differences in past history of the flow are important even though the local conditions at the measuring station are the same.

---

[9]From integration of the energy distribution across the boundary layer, conservation of energy is known to hold for Adcock and Peterson's adiabatic wall data.

In figures 18 and 19, stagnation temperature-velocity profiles in the correlation form $(T_t - T_w)/(T_{t,\infty} - T_w)$ versus u/U suggested by the Crocco energy equation are shown for the data previously presented against wall distance as well as data from several additional sources [28], [29], [30], [31], and [32]. In this type of plot, Crocco's equation for $N_{Pr} = 1$ gives a one-to-one correspondence between the two parameters and thus provides a convenient reference line to which the data can be compared. For cases where the y distances at which the temperature data were taken differed from those at which the velocity data were computed, faired values of u/U have been used. Figure 18 is composed of $M_\infty = 6.0$ data for several values of wall-to-stream stagnation temperature ratio while figure 19 contains data at different Mach numbers for two wall temperature cases, the adiabatic wall case and the $T_w/T_{t,\infty} \approx 0.5$ case. From these figures, it is seen that significant deviations from the Crocco values do occur, depending upon the Mach number and wall temperature. For the constant Mach number data of figure 18, Walz' theory is seen to qualitatively predict the trend of wall temperature, except for the overshoot in $T_t/T_{t,\infty}$ near the outer edge of the boundary layer for Adcock and Peterson's data. As previously discussed, no overshoot in $T_t/T_{t,\infty}$ would be expected for wall temperature significantly below adiabatic temperature, but an overshoot for the adiabatic case is expected.

In the adiabatic wall-temperature profiles of figure 19, the flat-plate incompressible data of Reynolds, Kays, and Kline[10] [29] are seen to be in excellent agreement with the Crocco equation. All of the compressible data show overshoots in $T_t/T_{t,\infty}$. Nothwang's flat-plate data [30] at $M_\infty = 3.0$ and Kistler's nozzle test section data [31] at Mach numbers of 1.7, 3.6, and 4.7 lie mostly above the Crocco line while that of Lobb, Winkler, and Persh is bowed considerably below the Crocco line as are also Adcock and Peterson's Mach 6.0 hollow cylinder data at intermediate values of u/U. Nothwang's and Kistler's data suggests a small downward trend with Mach number; however, there is a large unexplained difference between Kistler's Mach 4.7 data and the NOL Mach 4.9 data. Differences in past history of the flow or the fact that the NOL data were taken in a pressure gradient could be suspected for this behavior. However, as can be seen in figure 18 by visually noting the trend against wall-temperature ratio at the intermediate portion of the boundary layer, the Mach 6.0 hollow cylinder data (no pressure gradient) and the Mach 6.0 nozzle wall test section data (with previous pressure gradient history) seem to agree well with each other even though the velocity profiles were noted earlier to be significantly different. Also, the adiabatic wall hollow cylinder data at u/U values below about 0.85 and the Mach 4.9 NOL data agrees well with each other as well as Walz' theory, which is insensitive to Mach number.

For the $T_w/T_{t,\infty} \approx 0.5$ profiles of figure 19, it is noted that the nozzle-wall data tends to be significantly lower than the flat plate or hollow cylinder data. Here, it thus appears that past history of the flow has a pronounced effect upon the profiles. Within the intermediate portion of the boundary layer,

---

[10]The values of R_θ shown for this data were obtained using the Kármán-Schoenherr equation and the given values of R_x.

Danberg's Mach 6.4 flat-plate data [32] and Adcock and Peterson's Mach 6.0 hollow cylinder data are in good agreement with each other as well as Walz' theory. The NOL data [22], which covers Mach numbers from 5.1 to 8.2, shows no apparent effect of Mach number. The answer cannot be arrived at by the present superficial examination of the available data but will probably require a knowledge of the previous history of the boundary layer together with a sophisticated theory.

CONCLUDING REMARKS

Data from a large number of sources including flight and wind tunnel have been analyzed to provide information on the turbulent boundary layer at high speeds. Two of the obvious but important problems considered were the effect of Mach number and wall temperature on the heat transfer. In the supersonic speed range flight data had to be relied on to provide the trends at low wall-temperature ratios. The results were equivocal in that the data did not consistently support any one theory, though a trend of increasing heat transfer with decreasing wall temperature was indicated. For Mach numbers of about 5 and greater, there was found to be little effect of wall temperature on the heat-transfer level as predicted by the Spalding-Chi method. There was, however, a tendency for the Spalding-Chi method to underestimate the level of this heat transfer. There are indications that the Li-Nagamatsu theory, which takes into account the contribution of the density fluctuations to the shearing stress may account for the increased heating. The present experimental results do not allow a conclusive answer to this problem and definitive answers will probably have to await experiments at still higher Mach numbers than those presented in this paper.

The maximum heat transfer to flat plates and cones has also been examined. This maximum is closely represented by the peak in heating which has been used to designate the virtual origin of the boundary layer. For low-speed flow, momentum matching was found to give a good prediction of the experimental results on a flat plate. When properly ratioed to the results downstream of the virtual origin, the flat-plate peak heating ratios were apparently independent of Mach number at a value predicted for low-speed flow. The same ratio from cone experiments was lower than that given by the flat-plate experiments but also appeared to be essentially independent of Mach number.

Lastly, the structure of the boundary layer has been considered. Attempts to correlate the data in the simple form suggested by Crocco's integral of the energy-plus-momentum equation met with mixed results. For this type of plot, no definite trends with Mach number could be established, but a trend did appear to develop with wall-temperature variation which, in general, agreed with that predicted by Walz. Also, it was found that differences in past history of the flow had a pronounced effect upon the profiles even though the local conditions at the measuring station were the same.

In regard to the determination of skin friction from the often used velocity profile method, it was noted that it is difficult to obtain conclusive results, mainly because of the few data points usually available in the thin laminar sublayer region as well as probe interference effects near the wall. Examination of some published profiles along with the deduced skin-friction coefficients revealed that several of the skin-friction values could be significantly in error due to these difficulties.

APPENDIX A

BASIC EQUATIONS USED IN THE PAPER

Certain equations used in reducing and evaluating the data in this paper are included here for convenience and clarity.

Viscosity of air:

Keyes' proposed three constant empirical formula [33] was used

$$\mu = \frac{0.0232\, T^{3/2} \times 10^{-6}}{T + 220 \times 10^{-(9/T)}}, \frac{\text{lb-sec}}{\text{ft}^2} \tag{A1}$$

Kármán-Schoenherr incompressible skin friction formulas:

$$\frac{0.242}{\sqrt{C_{F,i}}} = \log_{10}\left(C_{F,i} R_x\right) = \log_{10}\left(2R_\theta\right) \tag{A2}$$

$$C_{f,i} = \frac{0.242 C_{F,i}}{0.242 + 0.8686\sqrt{C_{F,i}}} \tag{A3}$$

The Kármán form of Reynolds analogy factor [7]:

$$\frac{2N_{St,i}}{C_{f,i}} = \left\{1 + 5\sqrt{\frac{C_{f,i}}{2}}\left[\left(N_{Pr} - 1\right) + \log_e \frac{5N_{Pr} + 1}{6}\right]\right\}^{-1} \tag{A4}$$

The application of equation (A4) to equation (A3) to obtain $N_{St,i}$ is straightforward but the application to compressible flow is not. In applying the Kármán factor to compressible flow the particular theory was transformed to the incompressible plane. This was possible with the T-prime and Spalding-Chi methods. Then the Kármán factor corresponding to this incompressible (by transformation) value of C_f was used to change the compressible value of C_f to the compressible value of Stanton number. This was checked by plotting the Deissler-Loeffler [8] values for Reynolds analogy factor against the values of C_f transformed to incompressible flow by the method of Spalding-Chi (i.e., using the Spalding-Chi values of F_c and the Deissler-Loeffler value of C_f to obtain $F_c C_f$ where $F_c C_f$ is taken to be $C_{f,i}$). In this form the Deissler-Loeffler values of Reynolds analogy factor correlated remarkably well and were within 2 to 3 percent of the value given by Kármán. In applying the Kármán factor in this paper N_{Pr} was taken as 0.725.

APPENDIX B

TRANSFORMATION OF THE LOCAL SKIN FRICTION ON A TRUNCATED CONE TO THAT ON A POINTED CONE

If the local skin friction coefficient may be represented by the power law equation $C_f \propto R^{-1/n}$ then the transformation of distance on an axisymmetric body to that on a corresponding two-dimensional shape is given by Mangler [34] as

$$\bar{x} = \int_0^x \left(\frac{cr_o}{L}\right)^{\frac{n}{n-1}} dx \tag{B1}$$

$$\bar{y} = \frac{cr_o}{L}\, y \tag{B2}$$

The bar designates the quantities in two-dimensional flow; r_o is the local radius of the axisymmetric shapes; x is measured along a geodesic on the body; y is on a normal from the body surface. With $n = 2$, corresponding to laminar flow, the familiar exponent of 2 is obtained in equation (B1).

From equations (B1) and (B2) and the momentum equation one obtains the ratio of the local skin friction on a three-dimensional body to that in two-dimensional flow as

$$\frac{C_f\, R_v^{1/n}}{\bar{C}_f\, \bar{R}_v^{1/n}} = \left(\frac{cr_o}{L}\right)^{\frac{1}{n-1}} \left[\frac{x}{\int_0^x \left(\frac{cr_o}{L}\right)^{\frac{n}{n-1}} dx}\right]^{\frac{1}{n}} \tag{B3}$$

For the specific case of the ratio of the local skin friction on a truncated cone to that on a flat plate the result is

$$\frac{\left(C_f\, R_v^{1/n}\right)_{tc}}{\left(C_f\, R_v^{1/n}\right)_{fp}} = \left(\frac{2n-1}{n-1}\right)^{1/n} \left\{\left(1 + \frac{R_{l,p}}{R_v}\right) - \frac{R_{l,p}}{R_v}\left[\frac{R_{l,p}/R_v}{1 + \left(R_{l,p}/R_v\right)}\right]^{\frac{n}{n-1}}\right\}^{-1/n} \tag{B4}$$

or the ratio of the local skin friction on a truncated cone to that on a pointed cone is

$$\frac{\left(C_f\, R_v^{1/n}\right)_{tc}}{\left(C_f\, R_v^{1/n}\right)_c} = \left\{\left(1 + \frac{R_{l,p}}{R_v}\right) - \frac{R_{l,p}}{R_v}\left[\frac{R_{l,p}/R_v}{1 + \left(R_{l,p}/R_v\right)}\right]^{\frac{n}{n-1}}\right\}^{-1/n} \qquad \text{(B5)}$$

Equation (B5) with $n = 4$ was used to correct the turbulent cone data to correspond to that on a pointed cone with turbulent flow from the apex. The sketch below defines the Reynolds numbers shown in equations (B4) and (B5).

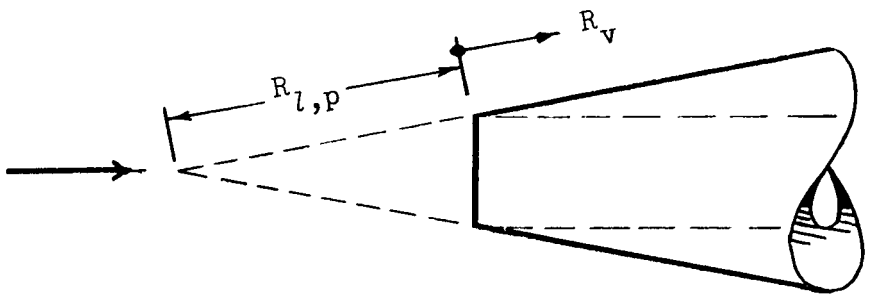

REFERENCES

1. Dhawan, S., and Narasimha, R.: Some Properties of Boundary Layer Flow During the Transition From Laminar to Turbulent Motion. Jour. of Fluid Mech., Vol. 3, No. 4, Jan. 1958, pp. 418-436.

2. Coles, Donald: Measurements of Turbulent Friction on a Smooth Flat Plate in Supersonic Flow. Jour. Aero. Sci., Vol. 21, No. 7, July 1954, pp. 433-448. (Also see JPL Report No. 20-71, 1953.)

3. Hakkinen, Raimo J.: Measurements of Turbulent Skin Friction on a Flat Plate at Transonic Speeds. NACA TN 3486, Sept. 1955.

4. Matting, Fred W., Chapman, Dean R., Nyholm, Jack R., and Thomas, Andrew G.: Turbulent Skin Friction at High Mach Numbers and Reynolds Numbers in Air and Helium. NASA TR R-82, 1960.

5. Bertram, Mitchel H.: Boundary-Layer Displacement Effects in Air at Mach Numbers of 6.8 and 9.6. NASA TR R-22, 1959. (Supersedes NACA TN 4133, 1958.)

6. Reynolds, W. C., Kays, W. M., and Kline, S. J.: Heat Transfer in the Turbulent Incompressible Boundary Layer. IV - Effect of Location of Transition and Prediction of Heat Transfer in a Known Transition Region. NASA MEMO 12-4-58W, Dec. 1958.

7. von Kármán, Th.: The Analogy Between Fluid Friction and Heat Transfer. ASME Trans., Vol. 61, No. 8, Nov. 1939, pp. 705-710.

8. Deissler, R. G., and Loeffler, A. L.: Analysis of Turbulent Flow and Heat Transfer on a Flat Plate at High Mach Numbers With Variable Fluid Properties. NACA TN 4262, April 1958.

9. Tetervin, Neal: A Semi-Empirical Derivation of Friction, Heat-Transfer, and Mass-Transfer Coefficients for the Constant Property Turbulent Boundary Layer on a Flat Plate. NOL TR 63-77, July 1963.

10. Bertram, Mitchel H.: Exploratory Investigation of Boundary-Layer Transition on a Hollow Cylinder at a Mach Number of 6.9. NACA Rep. 1313, 1957. (Supersedes NACA TN 3546, 1956.)

11. Van Driest, E. R.: Turbulent Boundary Layer on a Cone in a Supersonic Flow at Zero Angle of Attack. Jour. Aero. Sci., Vol. 19, No. 1, Jan. 1952, pp. 55-57, 72.

12. DeCoursin, D. G., Bradfield, W. S., and Sheppard, J. J.: Aerodynamic Heating and Heat Transfer Phenomena at Mach Numbers 2.7 Through 5.7. WADC Tech. Rept. 53-379, Feb. 1954.

13. Burbank, Paige B., and Hodge, Leon B.: Distribution of Heat Transfer on a 10° Cone at Angles of Attack From 0° to 15° for Mach Numbers of 2.49 to 4.65 and a Solution to the Heat-Transfer Equation That Permits Complete Machine Calculations. NASA MEMO 6-4-59L, June 1959.

14. Bertram, Mitchel H.: Correlation Graphs for Supersonic Flow Around Right Circular Cones at Zero Yaw in Air as a Perfect Gas. NASA TN D-2339, June 1964.

15. Rumsey, Charles B., and Lee, Dorothy B.: Measurements of Aerodynamic Heat Transfer and Boundary-Layer Transition on a 10° Cone in Free Flight at Supersonic Mach Numbers up to 5.9. NASA TN D-745, May 1961.

16. Rumsey, Charles B., and Lee, Dorothy B.: Measurements of Aerodynamic Heat Transfer and Boundary-Layer Transition on a 15° Cone in Free Flight at Supersonic Mach Numbers up to 5.2. NASA TN D-888, Aug. 1961.

17. Merlet, Charles F., and Rumsey, Charles B.: Supersonic Free-Flight Measurement of Heat Transfer and Transition on a 10° Cone Having a Low Temperature Ratio. NASA TN D-951, Aug. 1961.

18. Tendeland, Thorval: Effects of Mach Number and Wall-Temperature Ratio on Turbulent Heat Transfer at Mach Numbers From 3 to 5. NASA TR R-16, 1959. (Supersedes NACA TN 4236, 1958.)

19. Bertram, Mitchel H.: Calculations of Compressible Average Turbulent Skin Friction. NASA TR R-123, 1962.

20. Spalding, D. B., and Chi, S. W.: The Drag of a Compressible Turbulent Boundary Layer on a Smooth Flat Plate With and Without Heat Transfer. Jour. Fluid Mech., Vol. 18, Part I, Jan. 1964, pp. 117-143.

21. Winkler, Eva M., and Cha, Moon H.: Investigation of Flat Plate Hypersonic Turbulent Boundary Layers With Heat Transfer at a Mach Number of 5.2. NAVORD Rept. 6631, Sept. 1959.

22. Lobb, Kenneth R., Winkler, Eva M., and Persh, Jerome: NOL Hypersonic Tunnel No. 4 Results VII: Experimental Investigation of Turbulent Boundary Layers in Hypersonic Flow. NAVORD Rept. 262, Mar. 1955.

23. Hill, F. K.: Turbulent Boundary Layer Measurements at Mach Numbers From 8 to 10. The Physics of Fluids, Vol. 2, No. 6, Nov.-Dec. 1959, pp. 668-680.

24. Van Driest, E. R.: The Problem of Aerodynamic Heating. Aero. Eng. Rev., Vol. 15, No. 10, Oct. 1956, pp. 26-41.

25. Li, Ting-Yi, and Nagamatsu, H. T.: Effect of Density Fluctuations on the Turbulent Skin Friction on a Flat Plate at High Supersonic Speeds. Proceedings of the Second Midwestern Conf. on Fluid Mech. held at Ohio State University, Mar. 17-19, 1952. (Also see CIT Memo 11, Nov. 1952.)

26. Holloway, Paul F., and Sterrett, James R.: Effect of Controlled Surface Roughness on Boundary-Layer Transition and Heat Transfer at Mach Numbers of 4.8 and 6.0. NASA TN D-2054, April 1964.

27. Walz, A.: Compressible Turbulent Boundary Layers. International Symp. on the Mechanics of Turbulence, Marseilles, France, Aug. 28-Sept. 2, 1961, Centre National de la Reserche Scientifique, N. Y. Gordon and Breach, 1964, pp. 299-350.

28. Hill, F. K.: Boundary Layer Measurements in Hypersonic Flow. Jour. of the Aero. Sci., Vol. 23, No. 1, Jan. 1956, pp. 35-42.

29. Reynolds, W. C., Kays, W. M., and Kline, S. J.: Heat Transfer in the Turbulent Incompressible Boundary. I - Constant Wall Temperature. NASA MEMO 12-1-58W, 1958.

30. Nothwang, George J.: An Evaluation of Four Experimental Methods for Measuring Mean Properties of a Supersonic Turbulent Boundary Layer. NACA Rept. 1320, 1957. (Supersedes NACA TN 3721, 1956.)

31. Kistler, Alan L.: Fluctuation Measurements in Supersonic Turbulent Boundary Layers. BRL Report No. 1052, Aug. 1958.

32. Danberg, James E.: Characteristics of the Turbulent Boundary Layer With Heat and Mass Transfer at M = 6.7. NOL TR 64-99, Oct. 1964.

33. Keyes, F. G.: The Heat Conductivity, Viscosity, Specific Heat and Prandtl Number for Thirteen Gases. Project Squid, MIT Tech. Rept. 37, April 1952.

34. Mangler, W.: Boundary Layers With Symmetrical Air Flow About Bodies of Revolution. Goodyear Aircraft Corp. Report R-30-18, (Trans.) 1946.

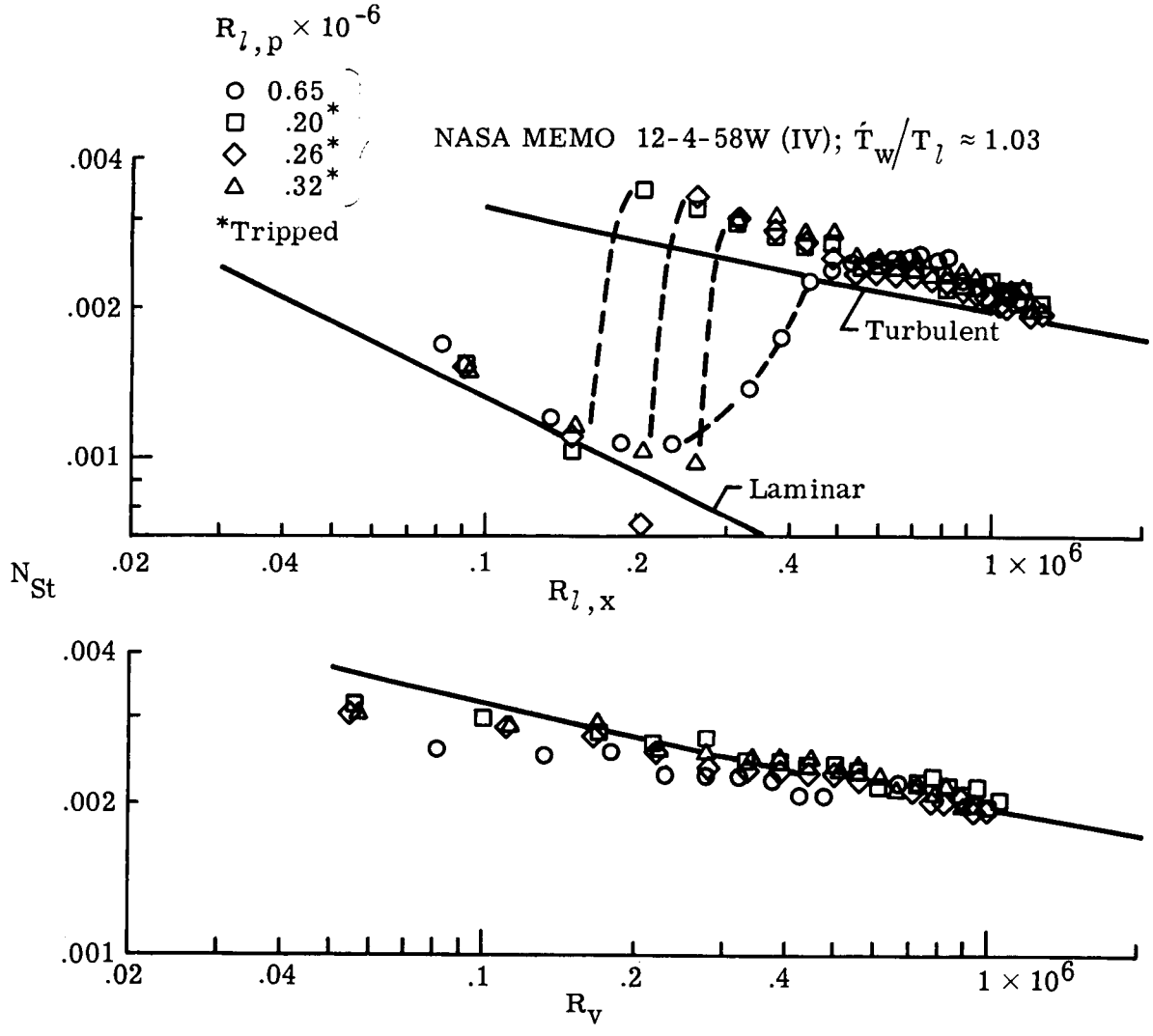

NASA

Figure 1.- Heat-transfer coefficients on a flat plate in low-speed flow as a function of Reynolds number from leading edge (upper) and Reynolds number from peak heat transfer (lower). Data from [6].

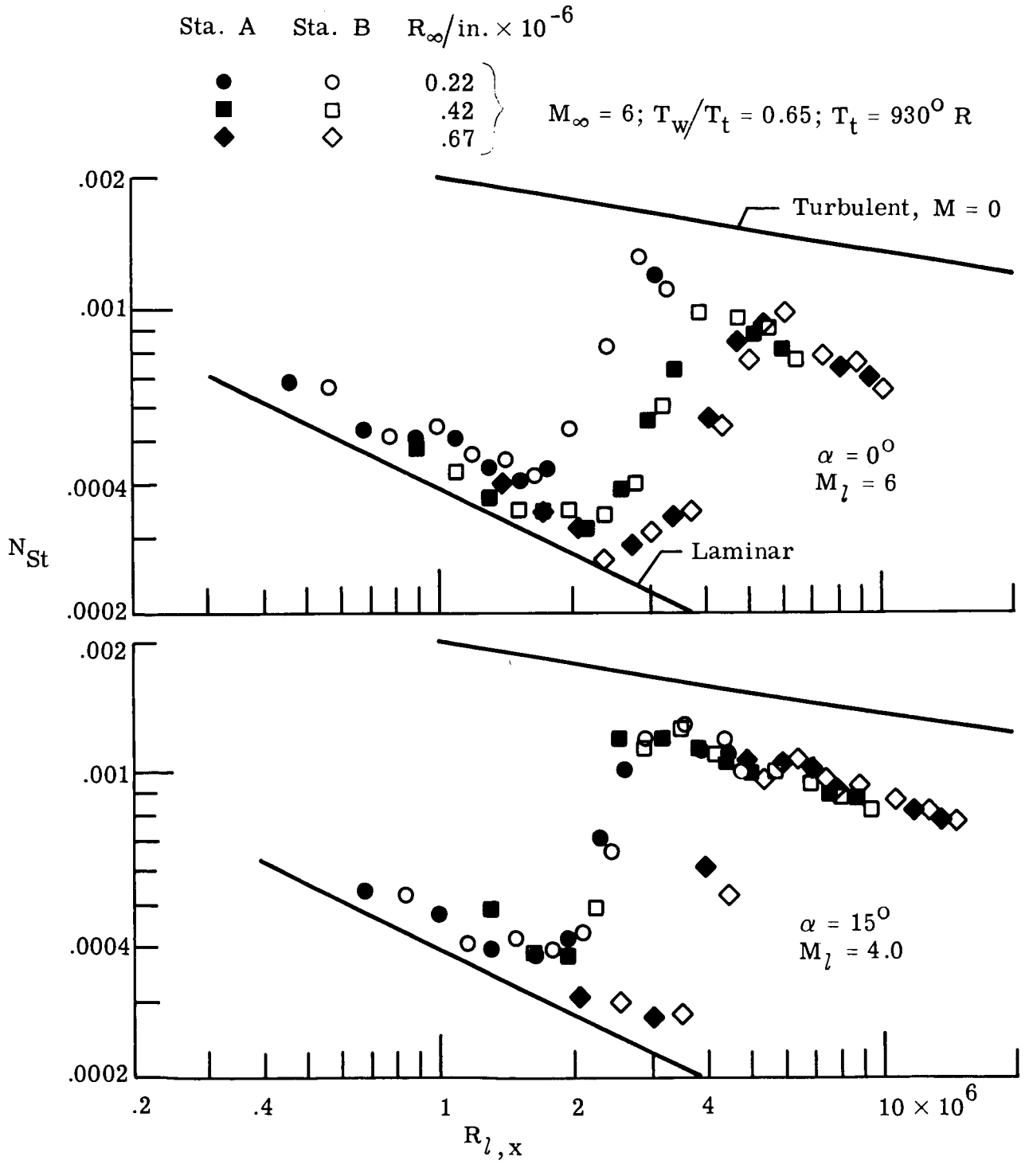

(a) Heat-transfer coefficients as a function of Reynolds number from leading edge. NASA

Figure 2.- Heat-transfer coefficients on a flat plate in a high-speed flow. Data from Langley 20-inch hypersonic tunnel; d = 0.002 in. (0.05 mm).

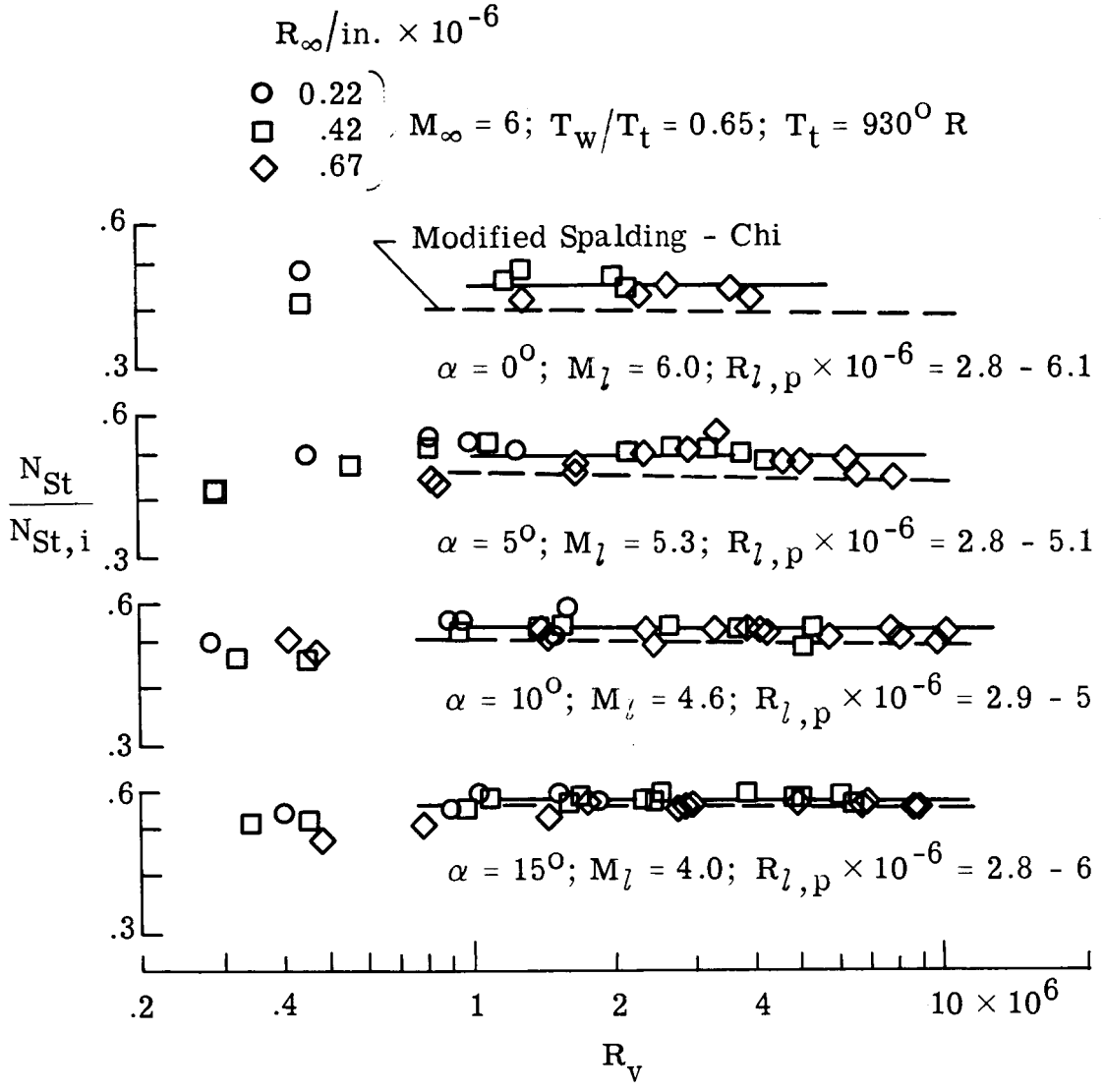

(b) Heat-transfer coefficients as a function of Reynolds number from peak heat transfer. NASA

Figure 2.- Concluded.

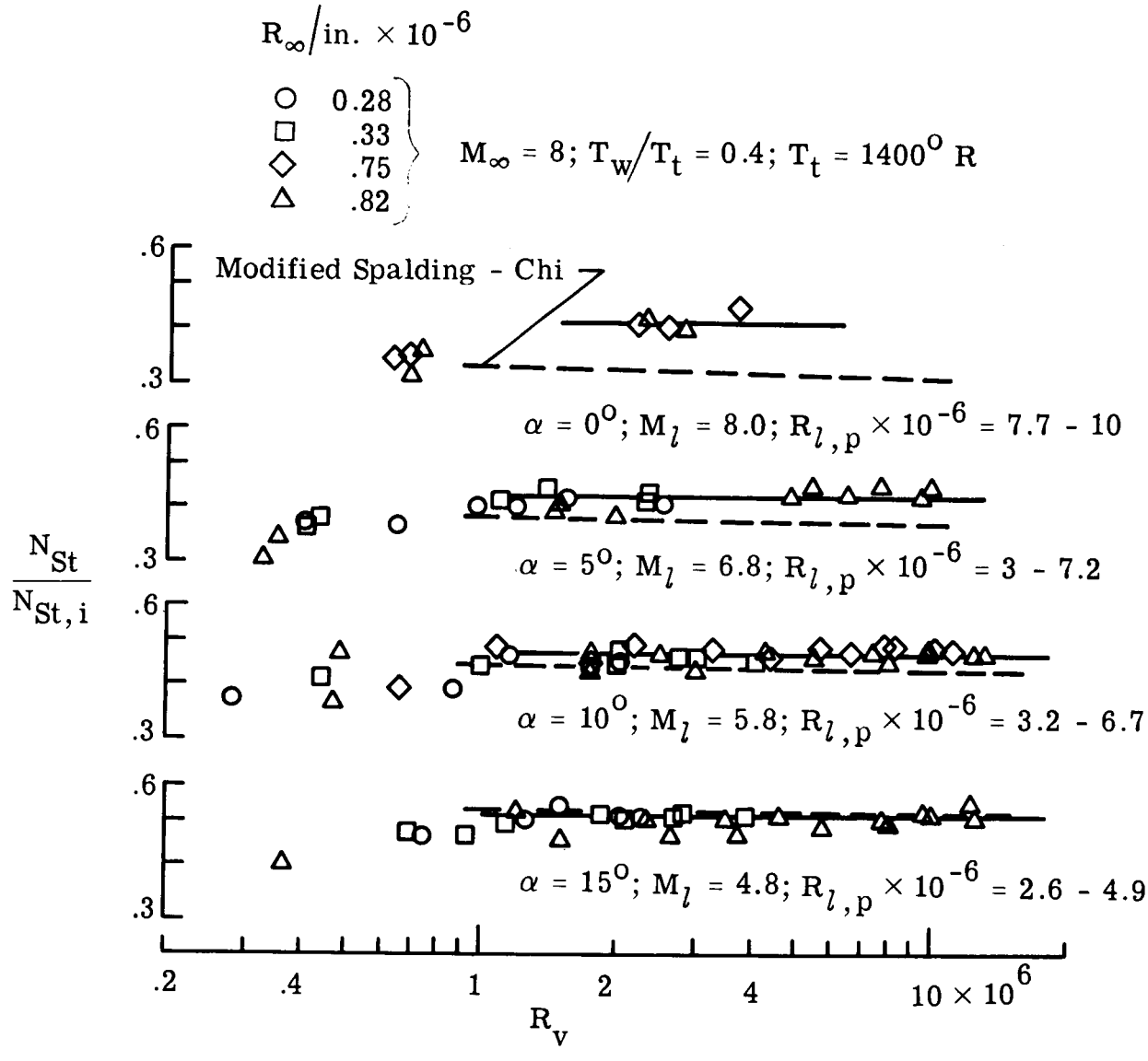

NASA

Figure 3.- Heat-transfer coefficients on a flat plate in a high-speed flow as a function of Reynolds number measured from peak heating. Data from Langley 18-inch variable-density wind tunnel; d = 0.002 in. (0.05 mm).

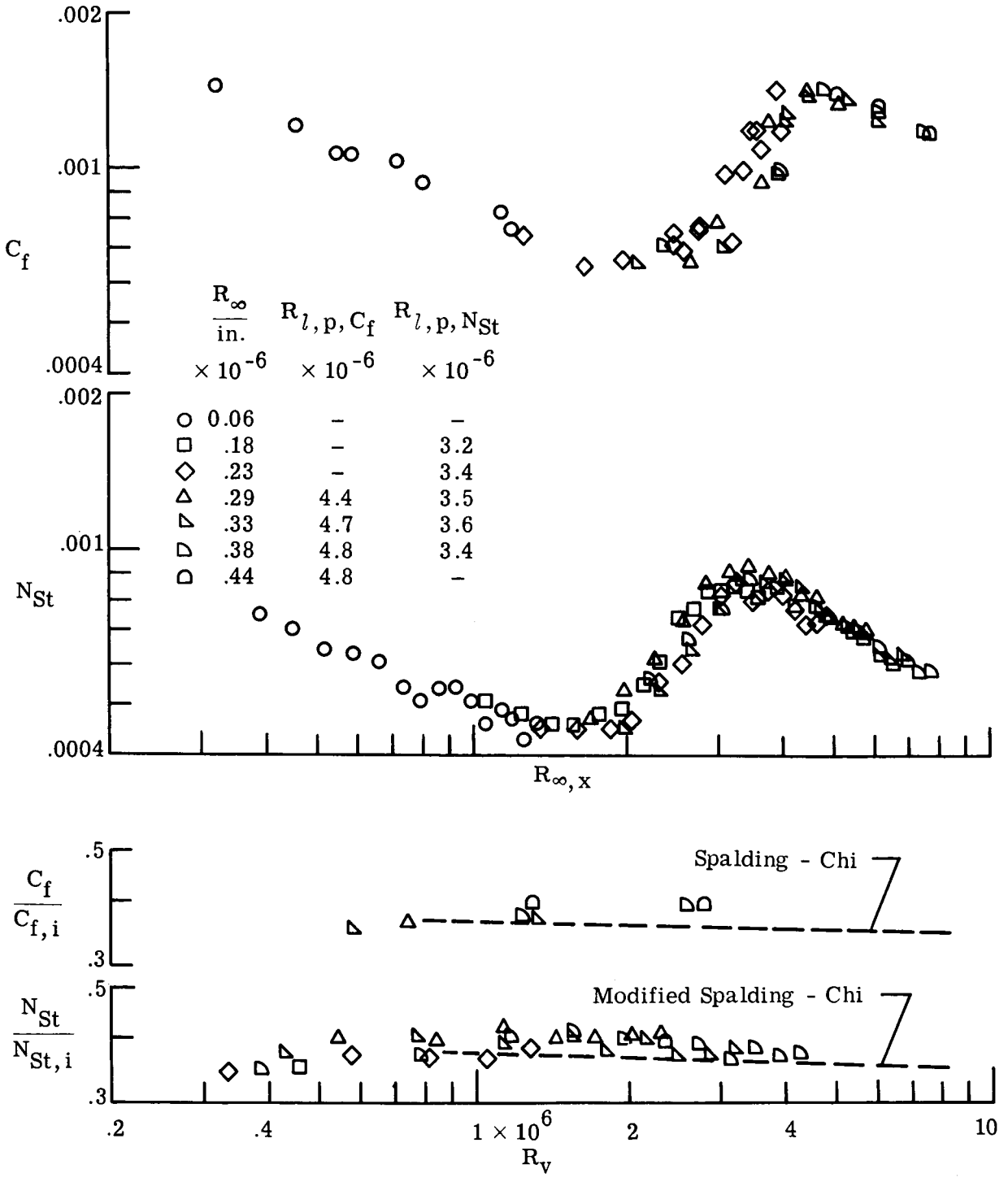

NASA

Figure 4.- Skin-friction and heat-transfer measurements on a flat plate in the Langley 11-inch hypersonic wind tunnel: $M_\infty = 6.8$; $T_w/T_t = 0.5$; $T_t = 1110^\circ$ R; d = 0.001 in. (0.025 mm).

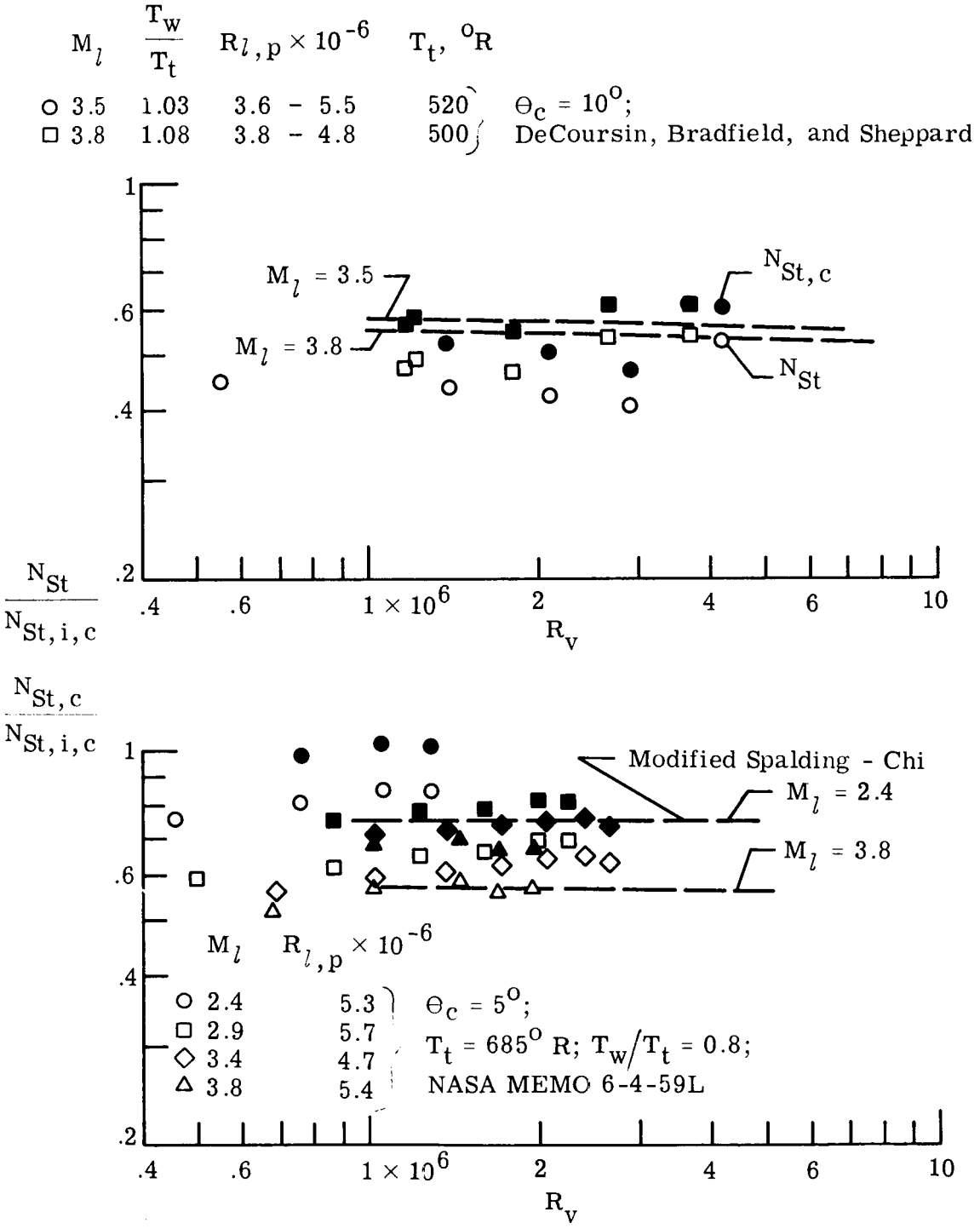

NASA

Figure 5.- Heat-transfer measurements on cones in supersonic wind-tunnel flow. Open symbols - original data (N_{St}); filled symbols - data modified to case where flow is turbulent from cone apex $(N_{St,c})$.

M_l	t, sec	$R_{l,p} \times 10^{-6}$	h_w / h_t	θ_c, deg	
1.79	14	7.1	1.3	5	NASA TN D-951
1.96	12	11.2	1.2		
3.01	5	40.8	.60		
3.15	4.5	45.2	.55		
3.28	3	46.0	.38		
3.31	4	48.8	.47		
3.48	3.5	56.0	.40		
3.6	19	9.0	.77	5	TN D-745
3.6	18	14.0	.73		
3.7	16	25.2	.59		
3.8	14.8	15.0	.44		
3.8	17.5	22.5	.40	7.5	TN D-888
3.8	17.75	24.0	.46		

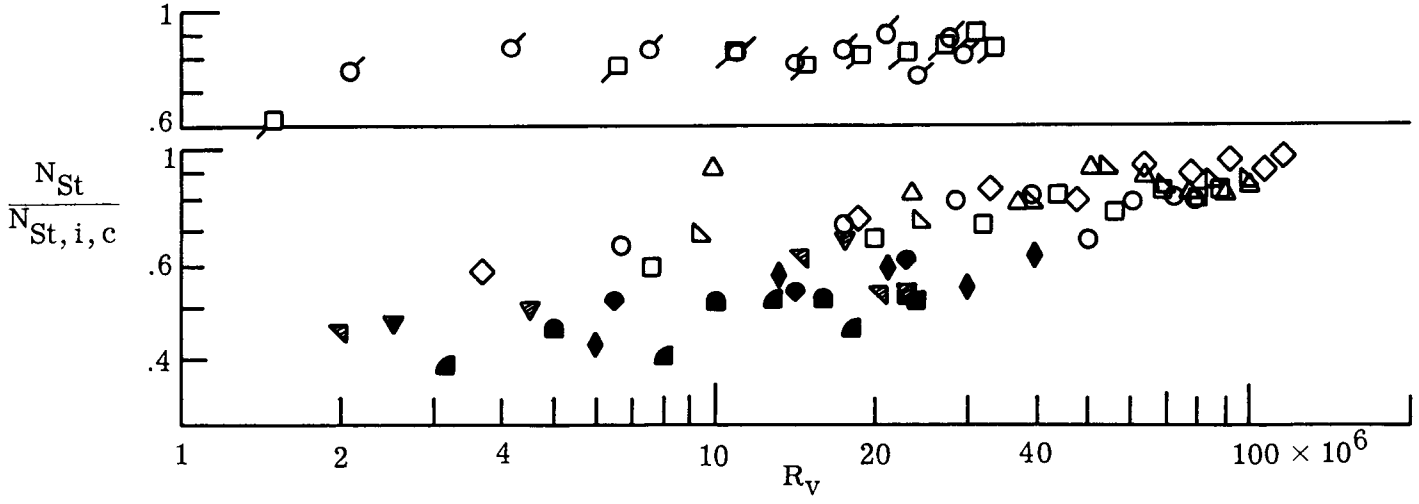

(a) Original data.

NASA

Figure 6.- Heat-transfer measurements on cones in supersonic flight.

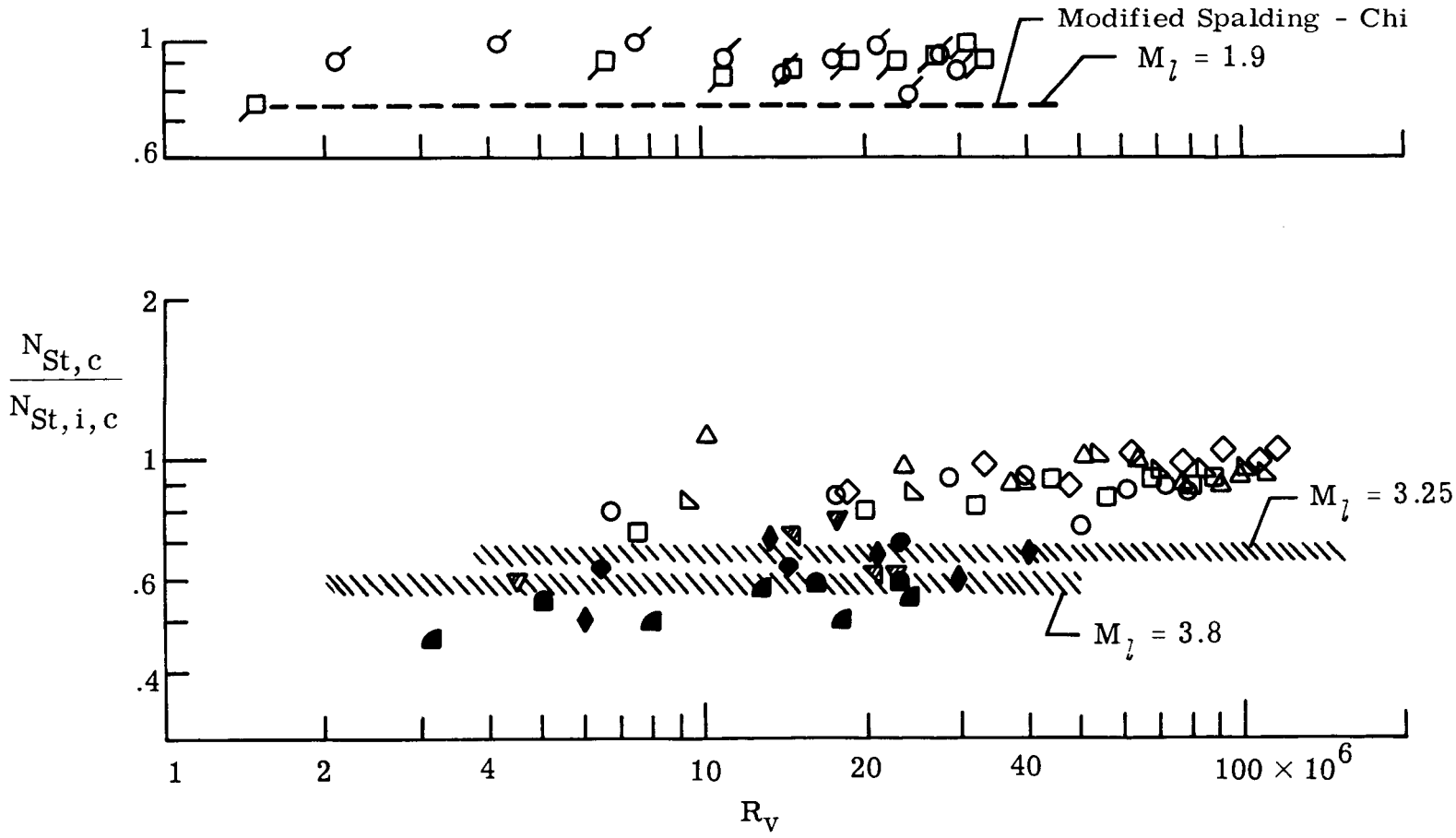

(b) Data modified to case where flow is turbulent from cone apex. NASA

Figure 6.- Concluded.

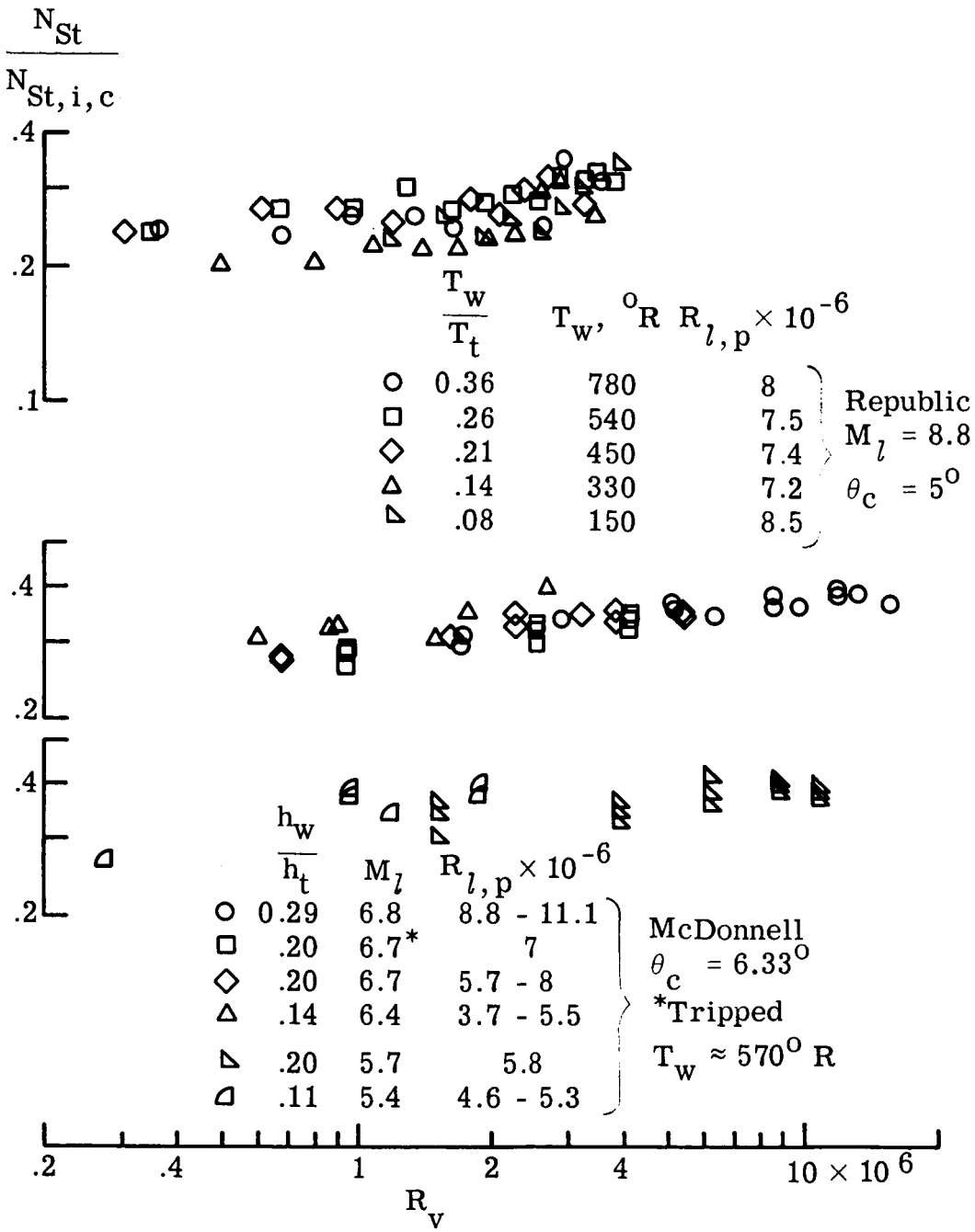

(a) Original data.

NASA

Figure 7.- Heat transfer on highly cooled cones in hypersonic flow. Data from Republic Aviation Corp. and McDonnell Aircraft Corp.

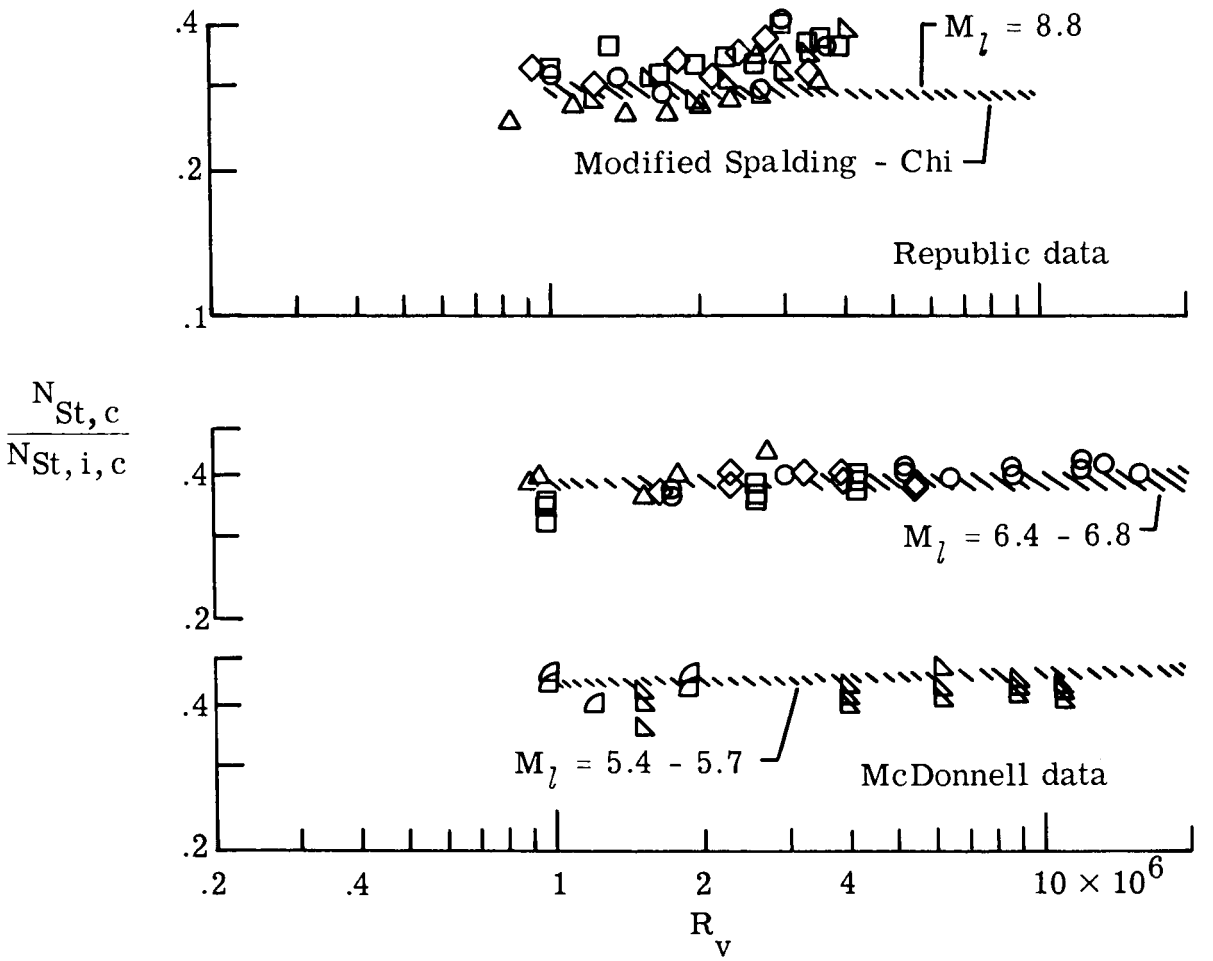

(b) Data modified to case where flow is turbulent from cone apex. NASA

Figure 7.- Concluded.

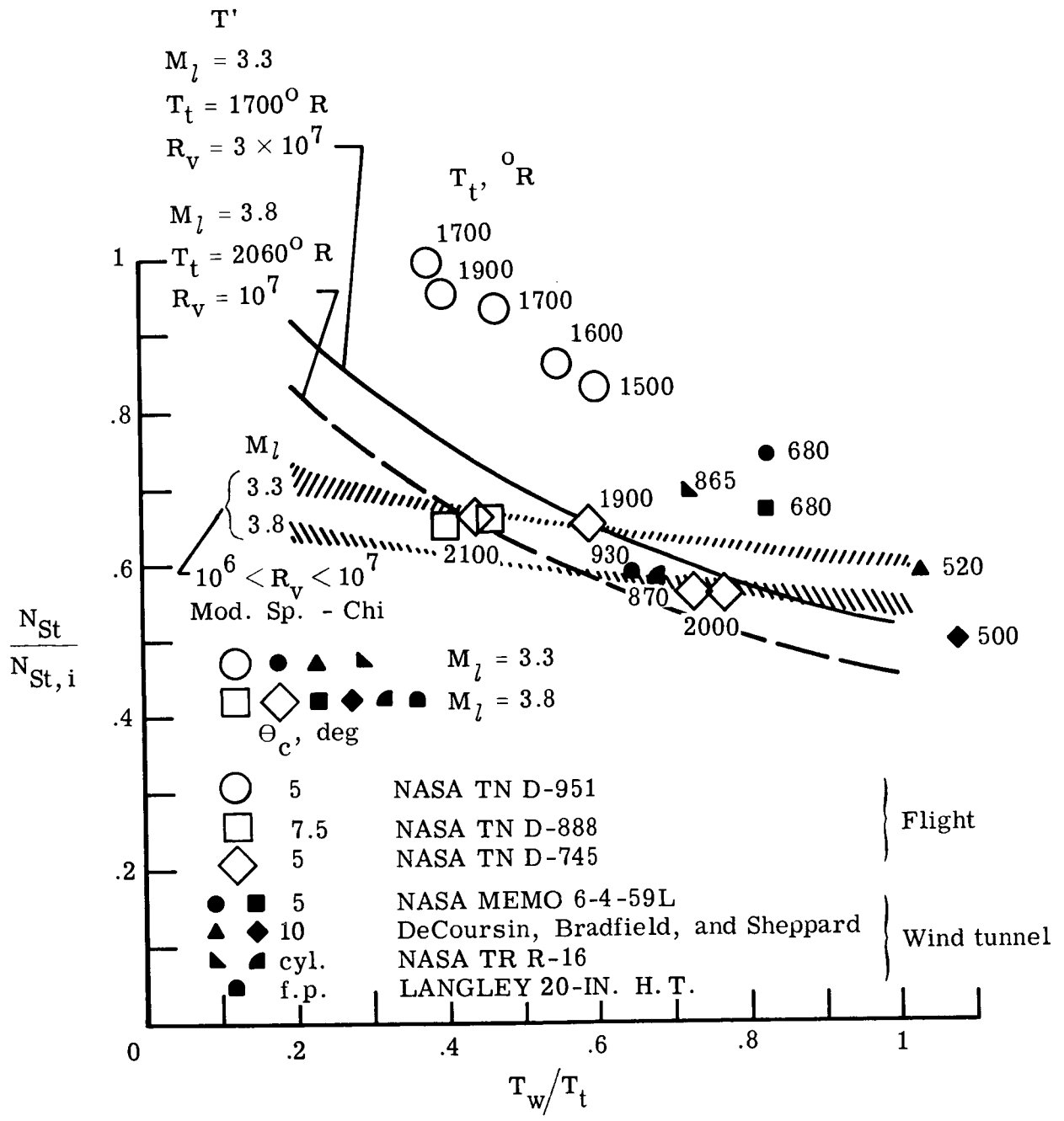

NASA

Figure 8.- Heat-transfer-coefficient ratio as a function of wall temperature ratio from flight and wind-tunnel experiments in supersonic flow and as given by two prediction methods.

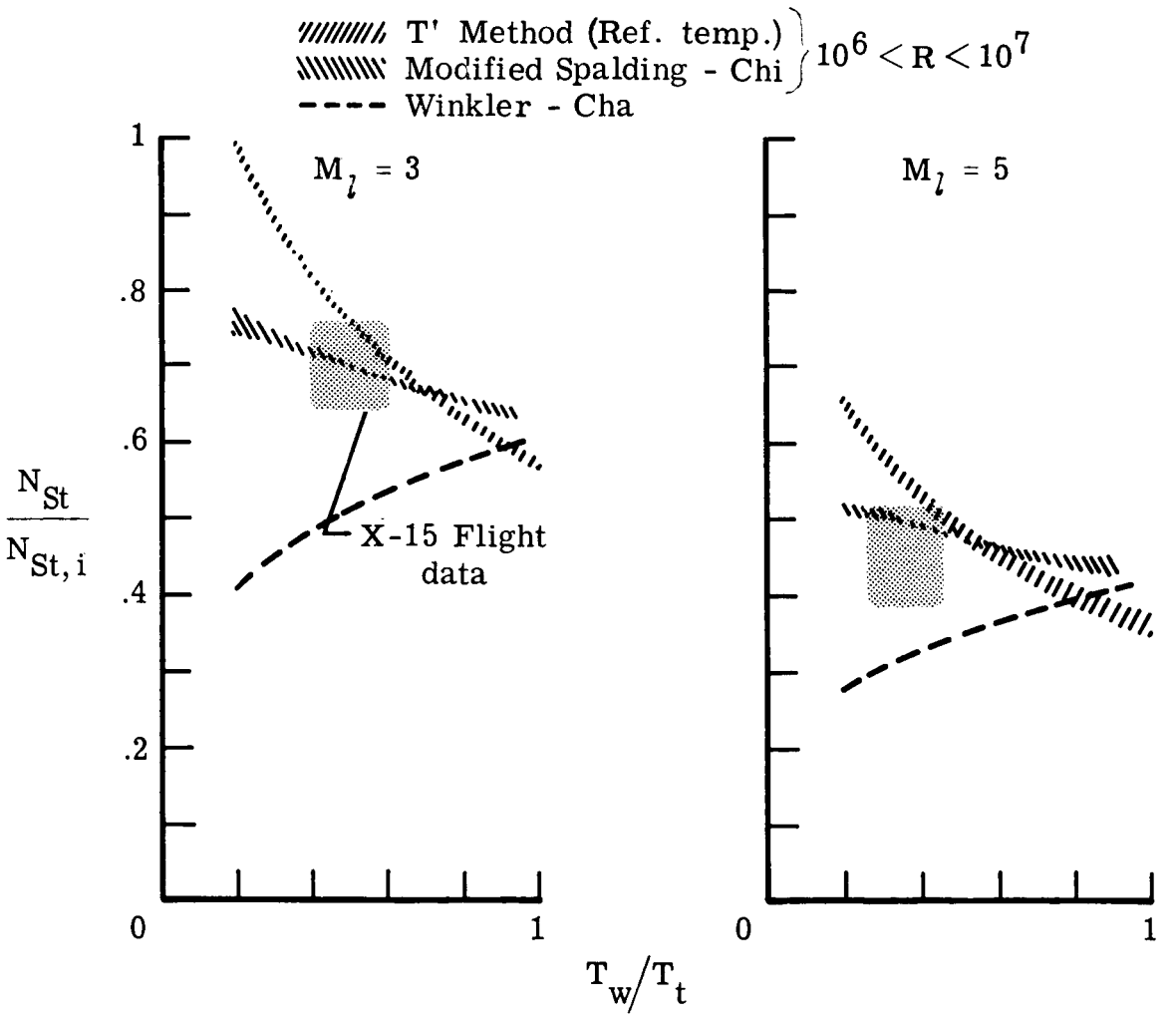

NASA

Figure 9.- Heat-transfer results from X-15 flights.

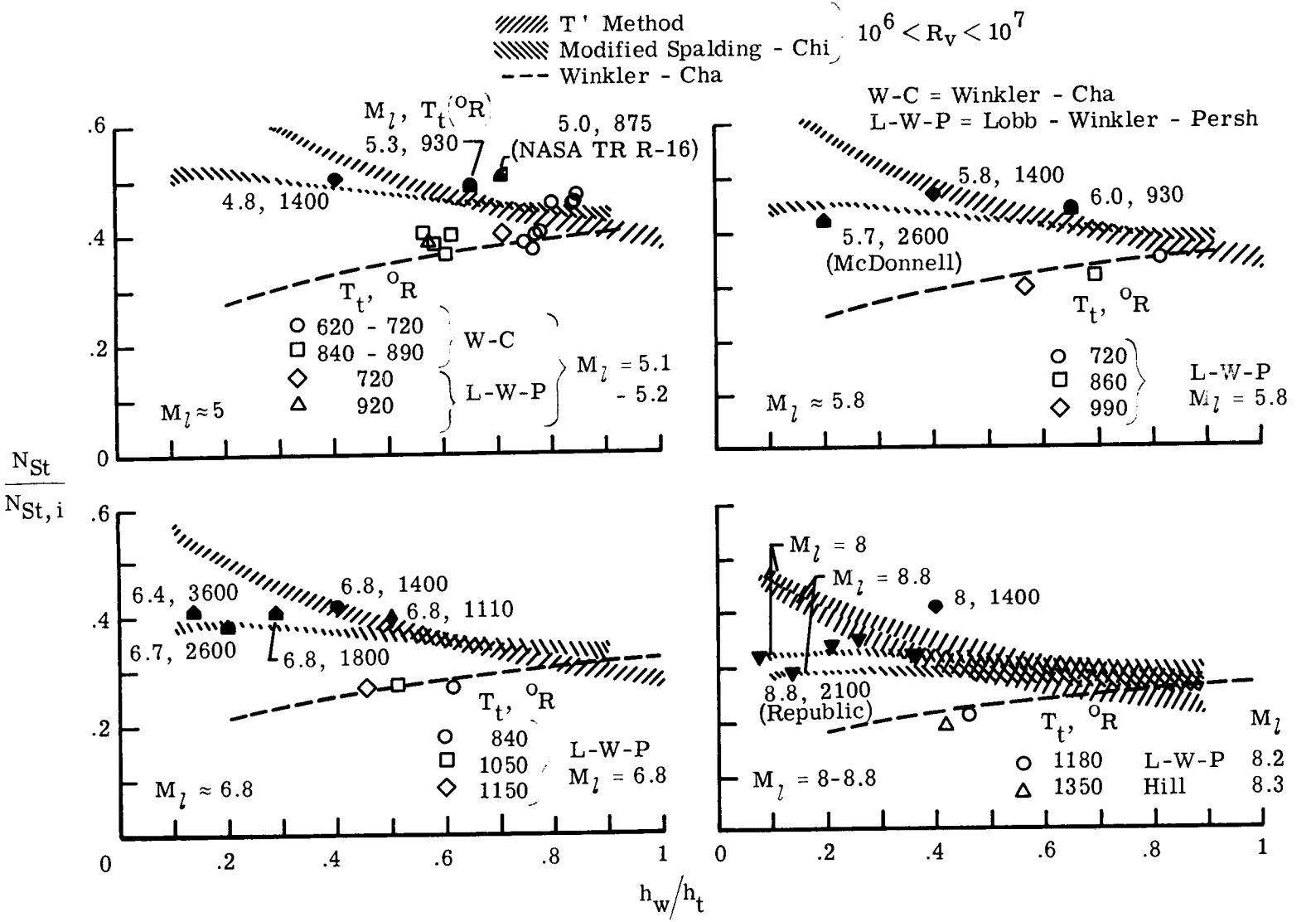

NASA

Figure 10.- Heat-transfer coefficient ratio as a function of wall temperature (enthalpy) ratio in hypersonic flow.

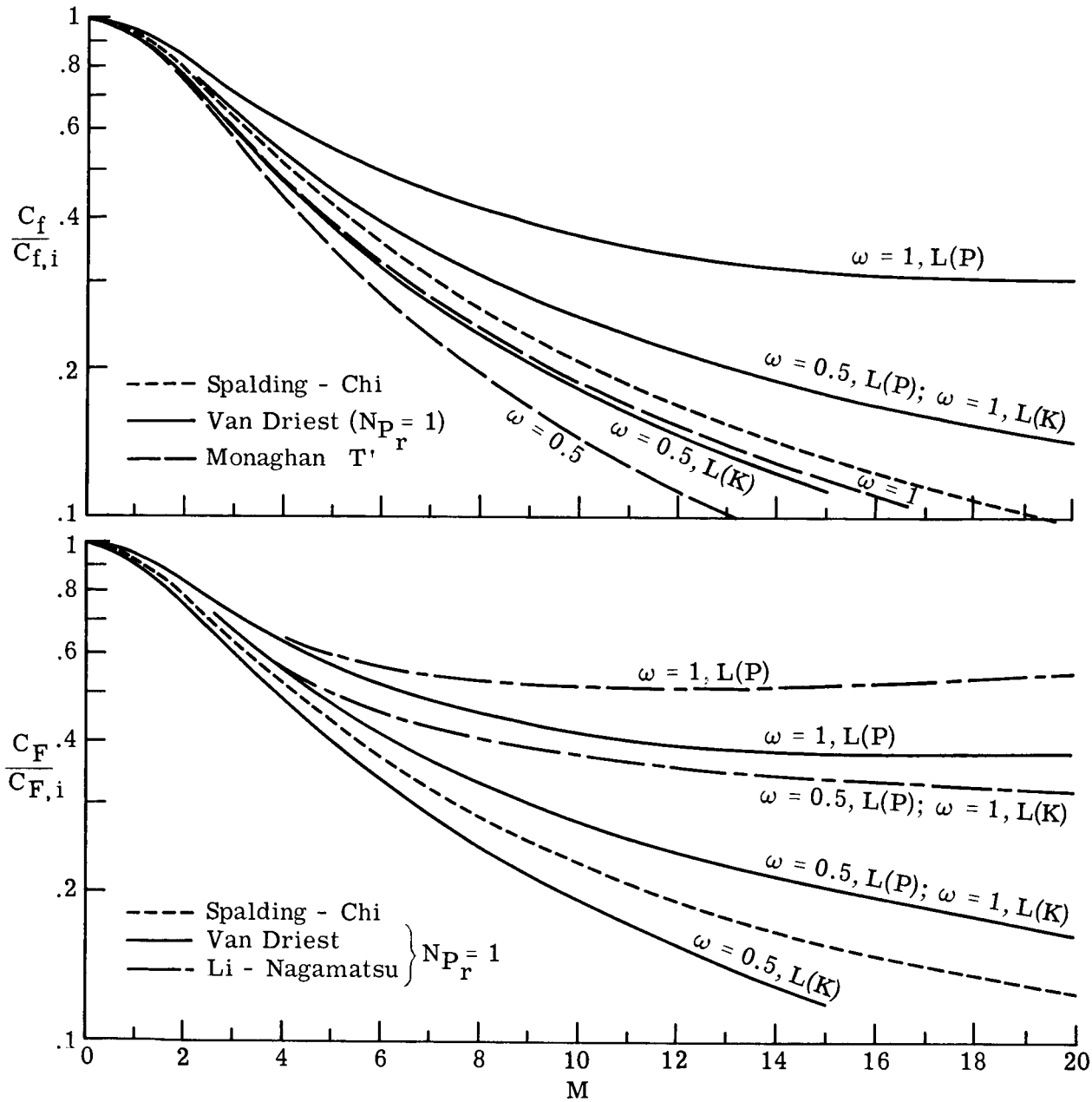

NASA

Figure 11.- Local and average skin-friction ratios as a function of Mach number as predicted by various theories; Reynolds number of 10^7.

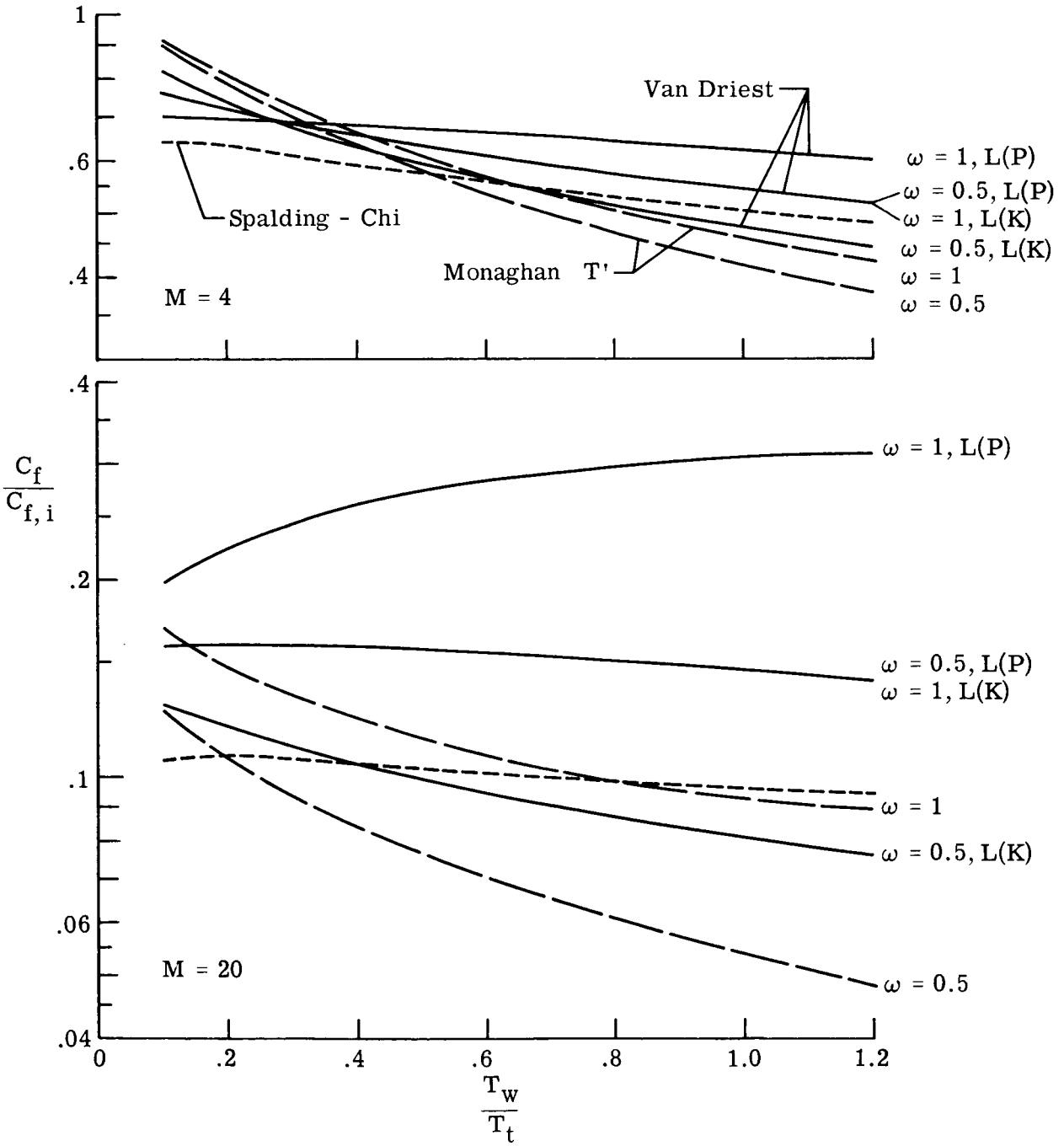

NASA

Figure 12.- Various predictions of the effect of wall temperature on local skin friction; Reynolds number of 10^7.

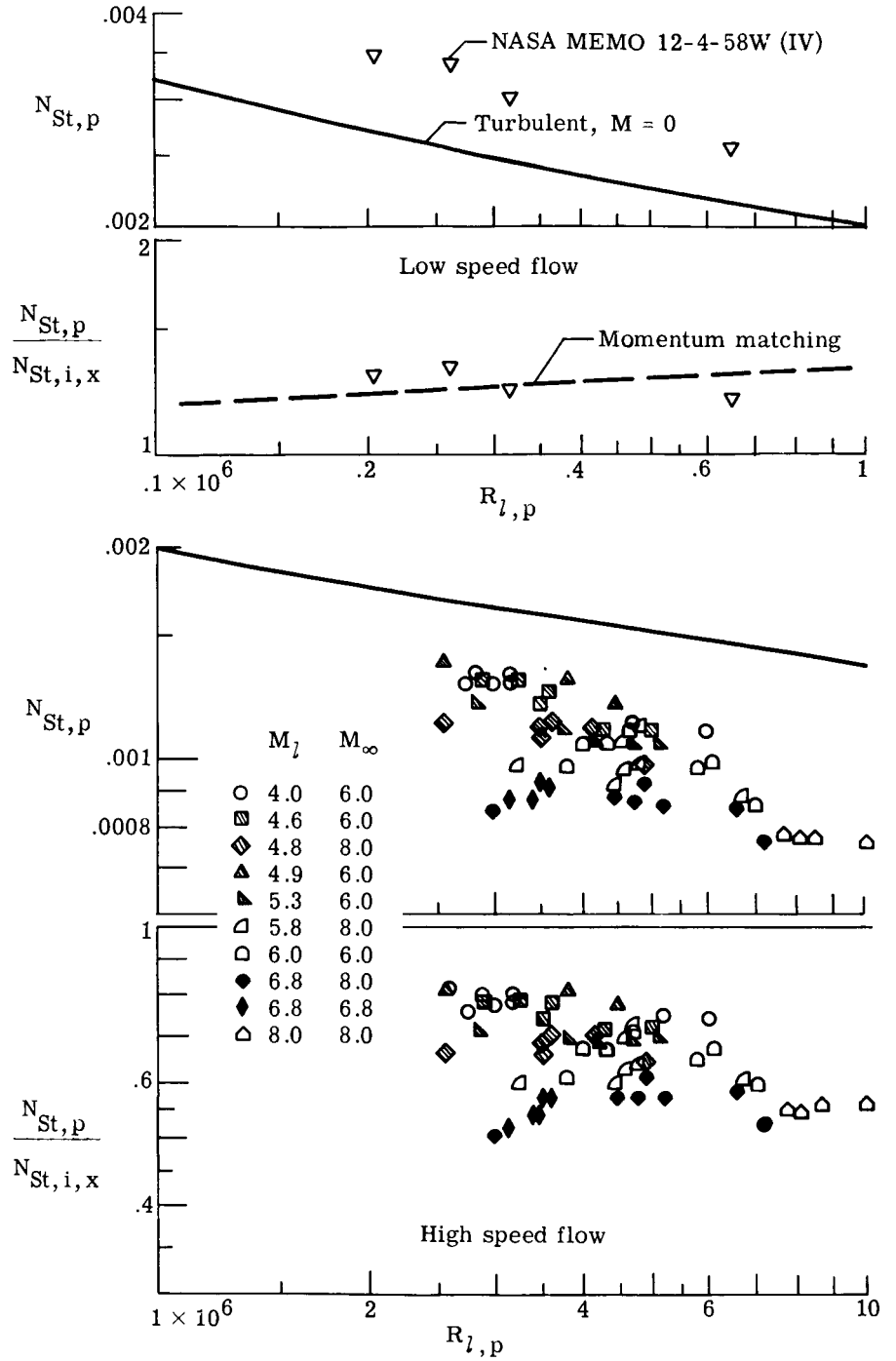

NASA

Figure 13.- Peak heating results on smooth flat plates. High-speed data from NASA Langley Research Center wind tunnels. See figures 2, 3, and 4 for conditions of tests.

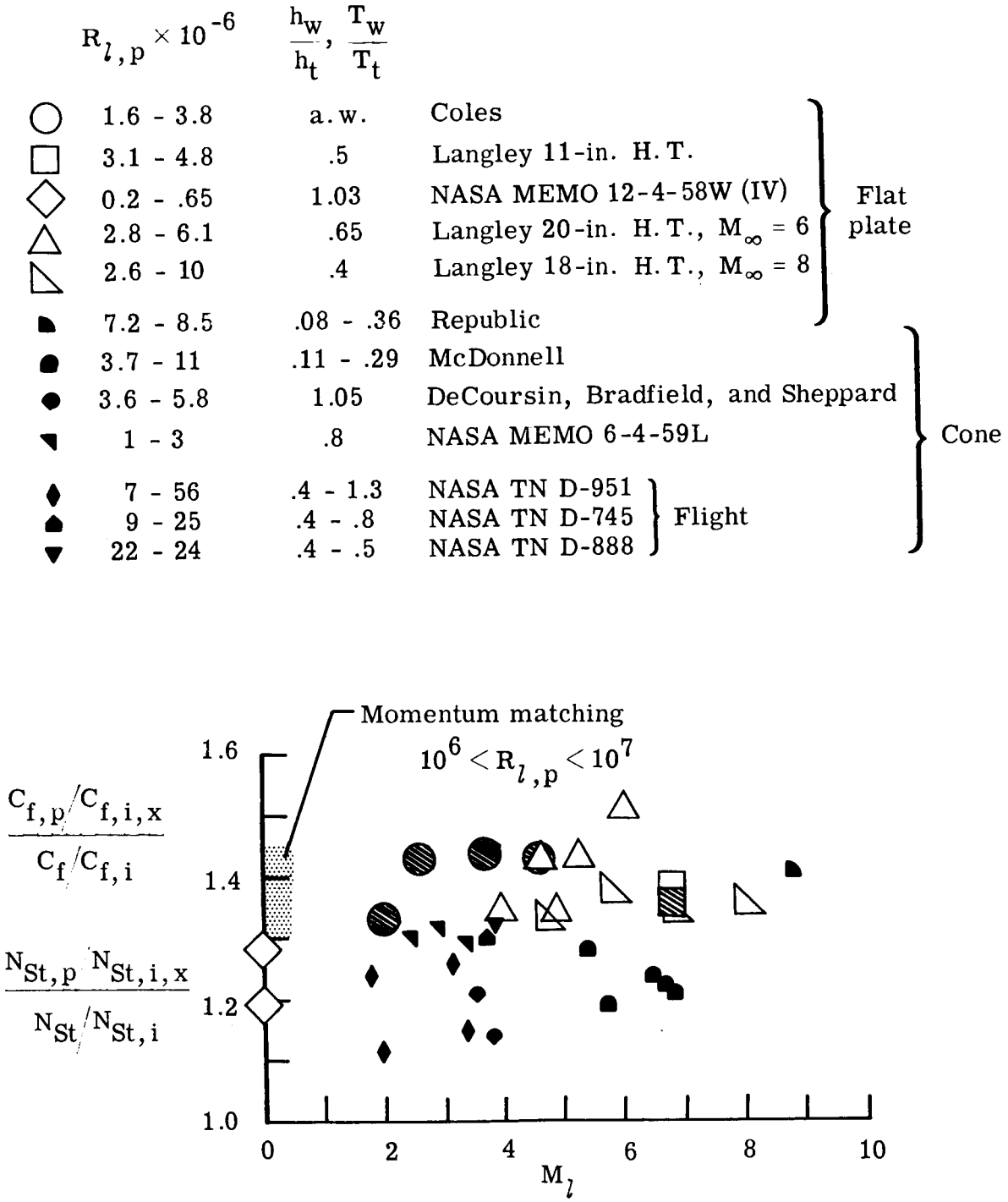

NASA

Figure 14.- Peak heating (or skin-friction) ratio divided by the heating (or skin-friction) ratio downstream of the virtual origin as a function of Mach number. Shaded symbols - skin-friction data; open and solid symbols - heat-transfer data.

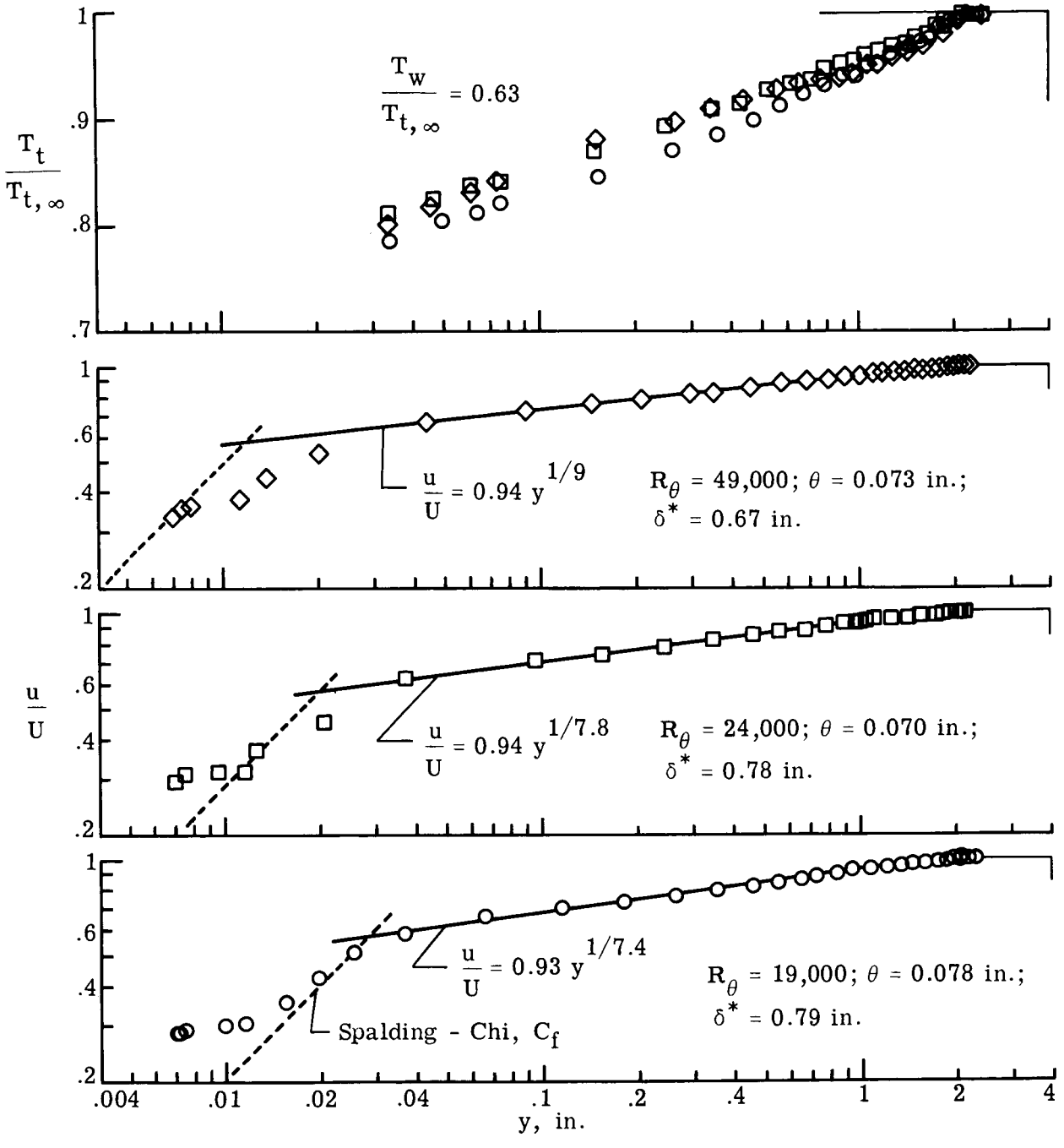

(a) $M_\infty = 6$; profiles on the test-section wall of the Langley 20-inch NASA hypersonic tunnel (two-dimensional contoured nozzle).

Figure 15.- Velocity and temperature profiles obtained in thick turbulent boundary layers growing on nozzle walls.

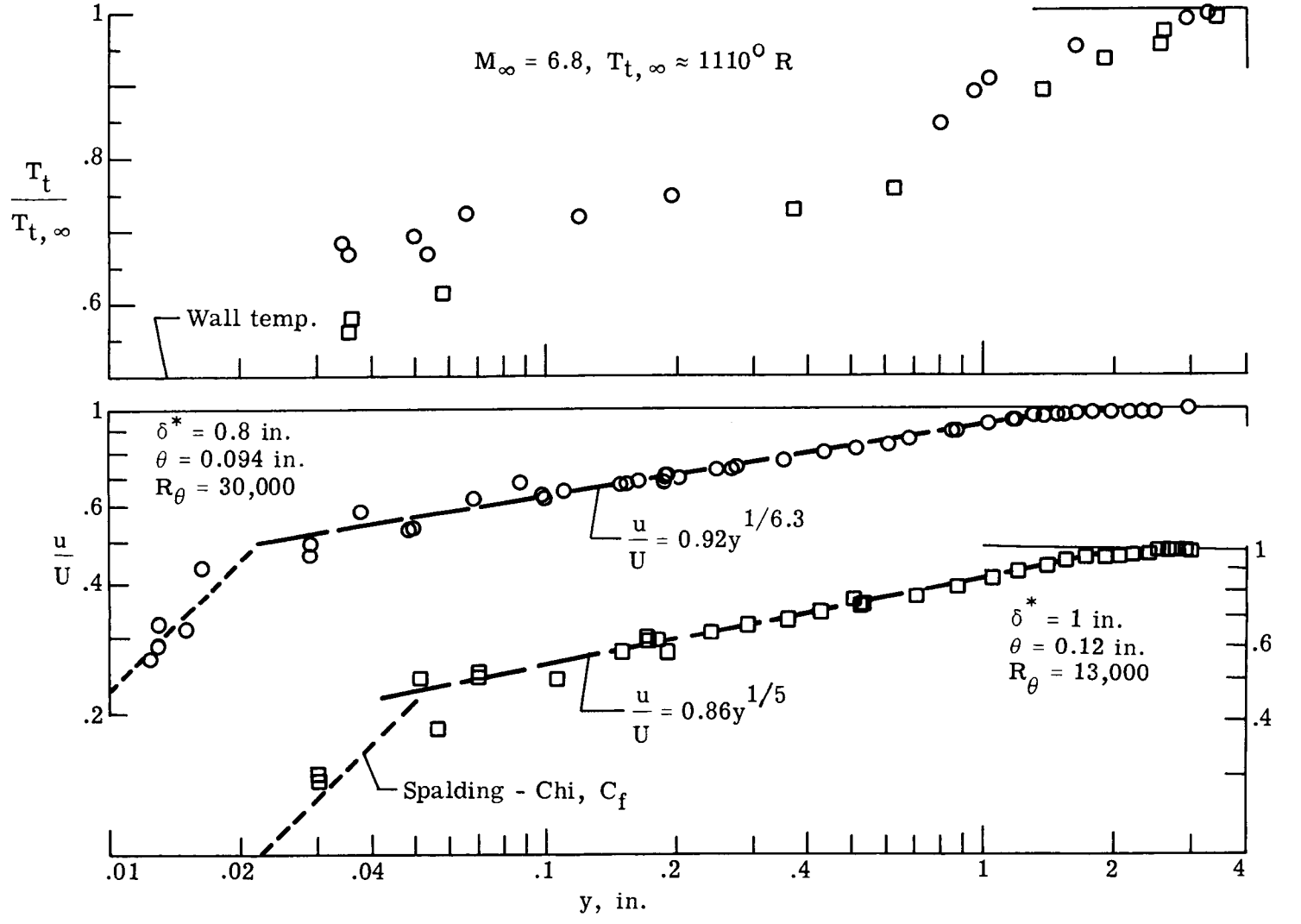

NASA

(b) $M_\infty = 6.8$; profiles on the test-section wall of the Langley 11-inch hypersonic tunnel (two-dimensional contoured nozzle).

Figure 15.- Continued.

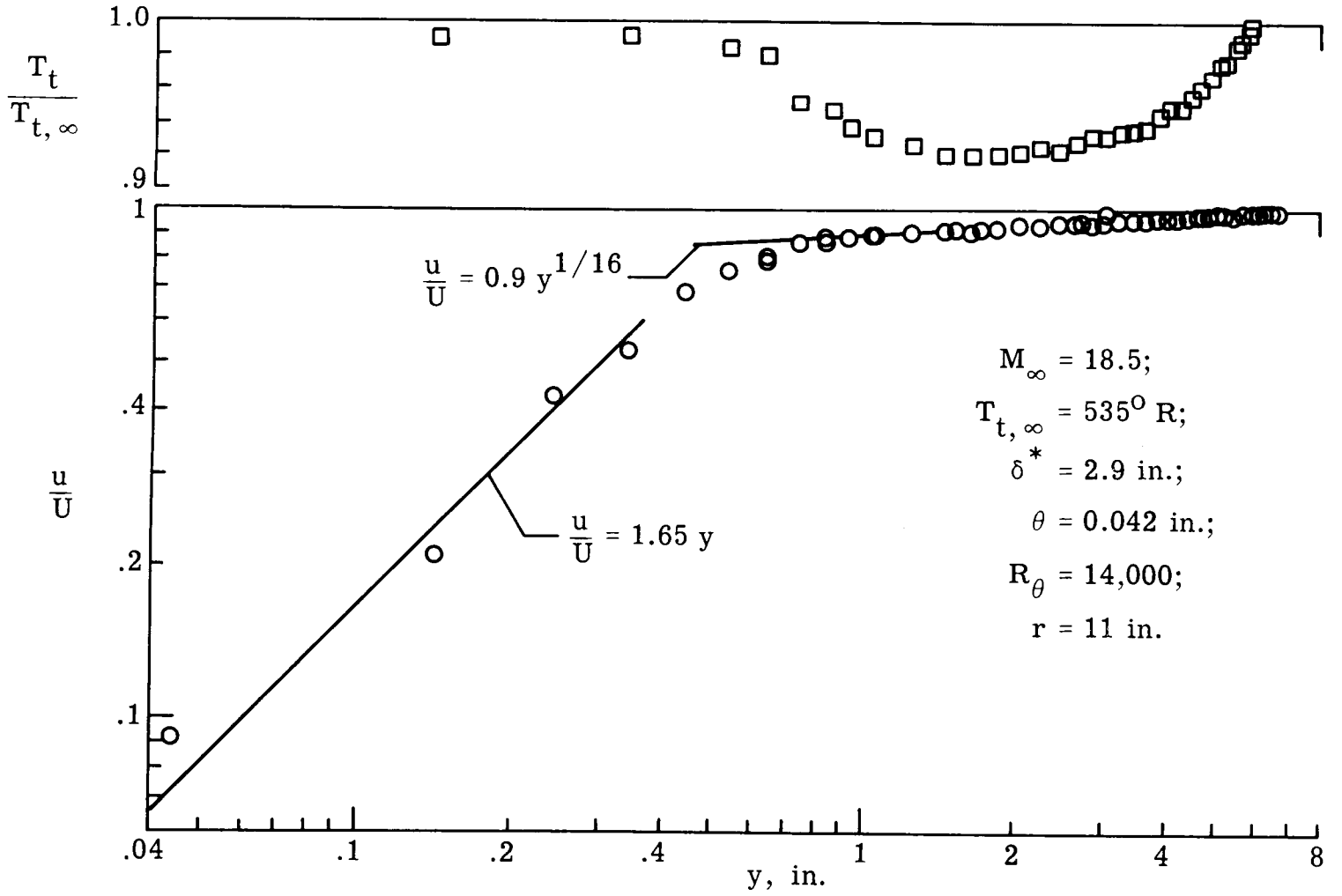

NASA

(c) $M_\infty = 18.5$; profiles on the test-section wall of the Langley 22-inch helium tunnel (axisymmetric contoured nozzle).

Figure 15.- Concluded.

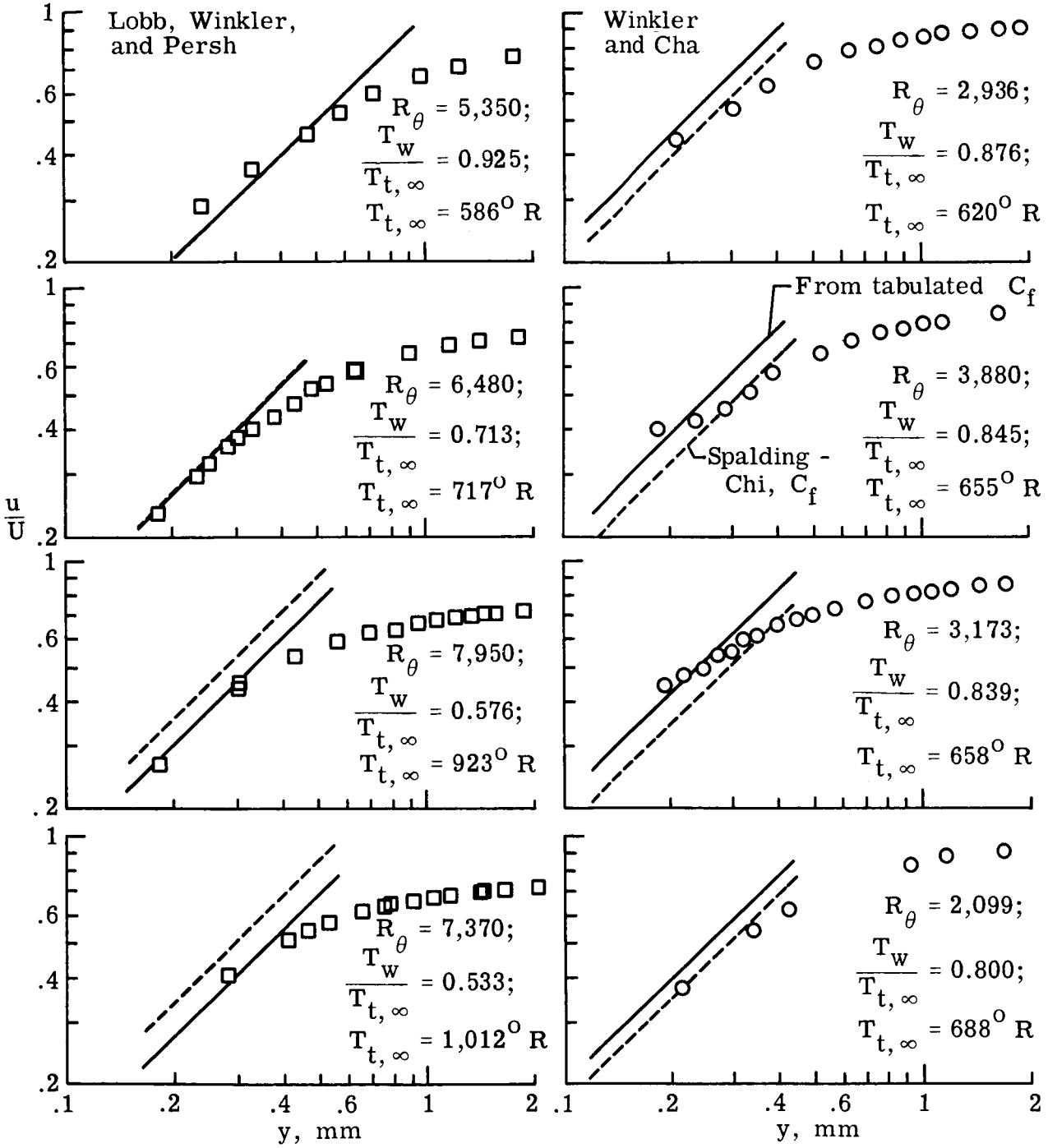

NASA

Figure 16.- Representative velocity profiles for Mach numbers near 5 from [21] and [22] for the inner region of the boundary layer.

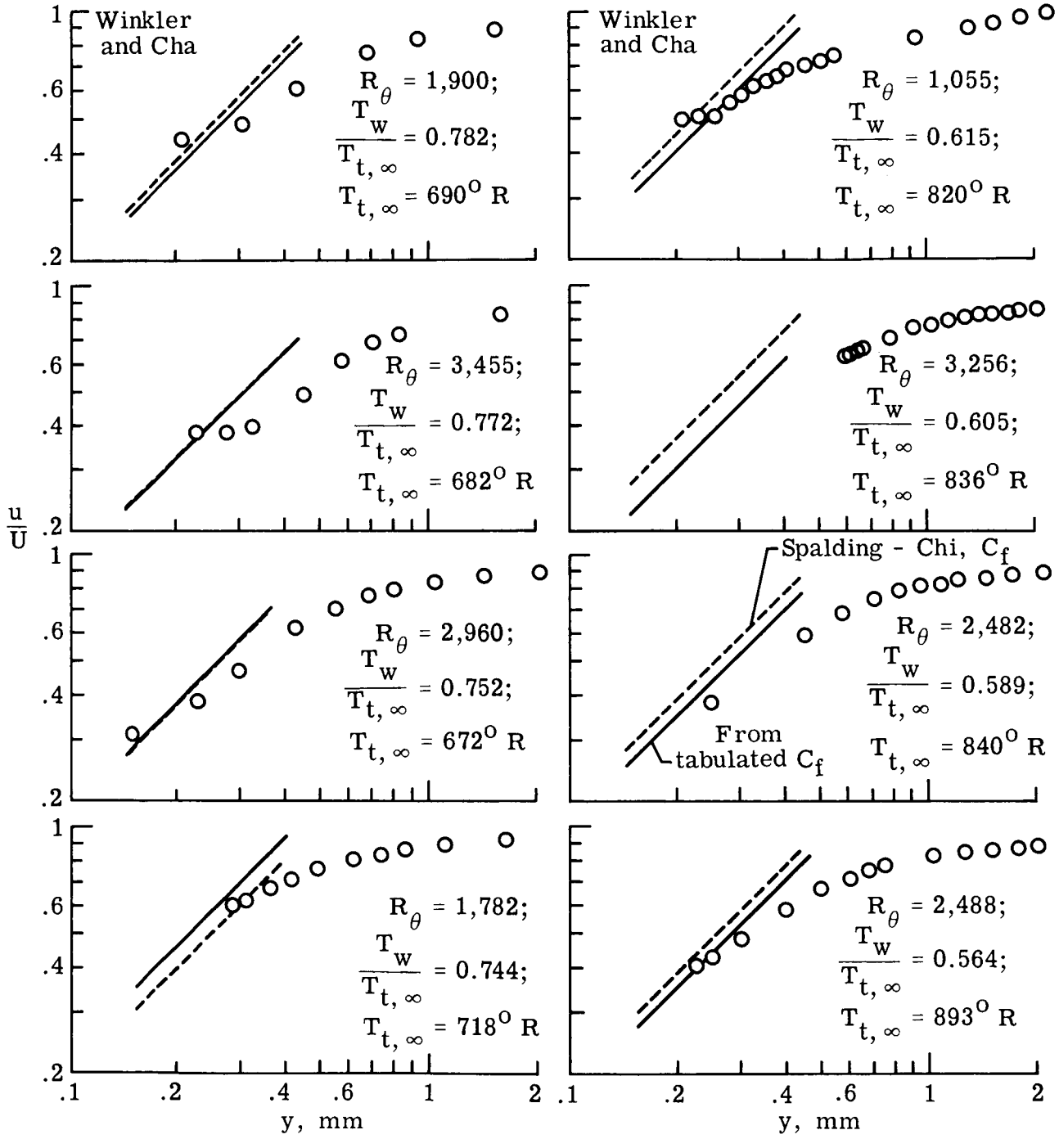

NASA

Figure 16.- Concluded.

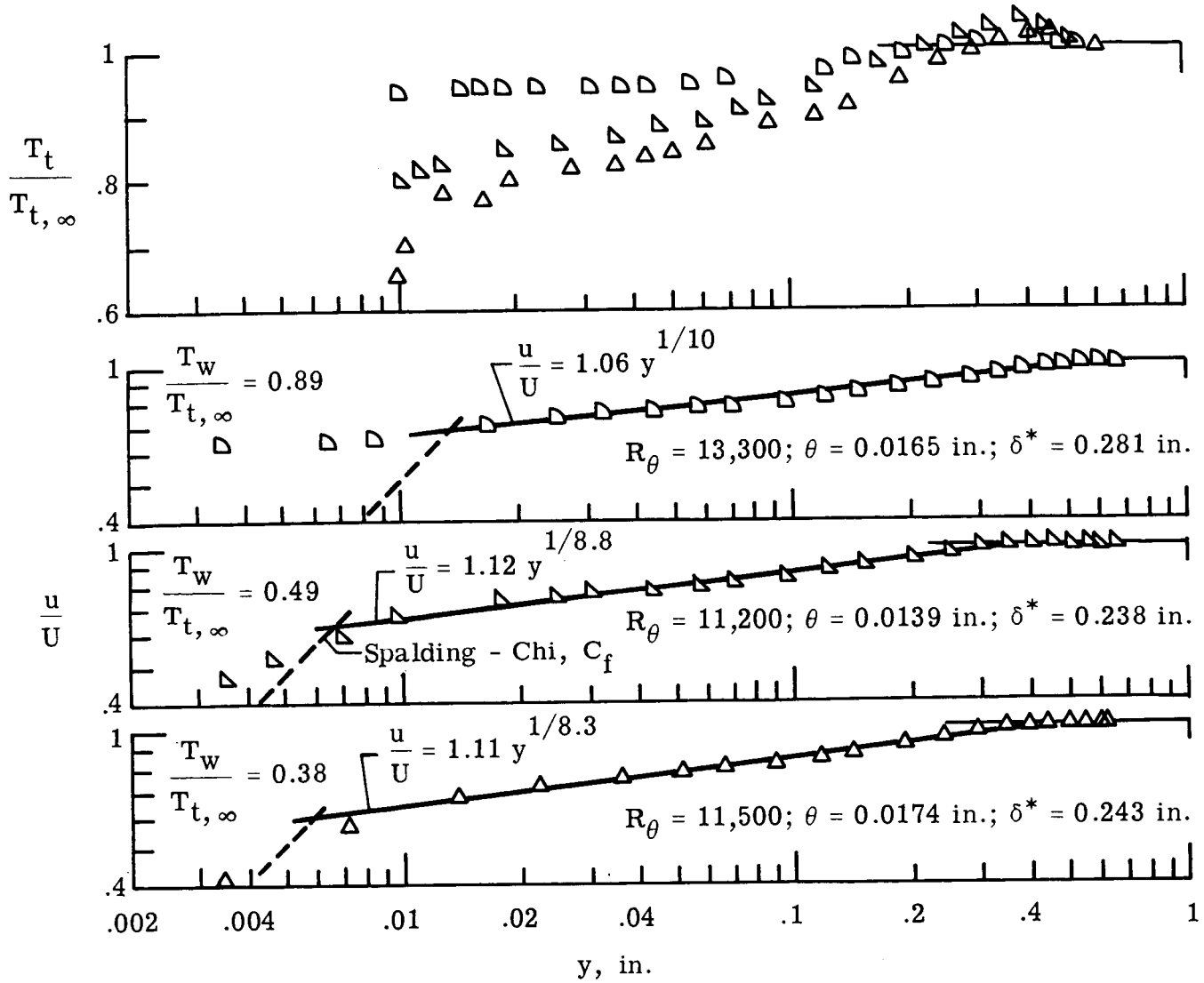

NASA

Figure 17.- Velocity and temperature profiles at $M_\infty = 6$ obtained on a hollow cylinder model in the Langley 20-inch hypersonic tunnel.

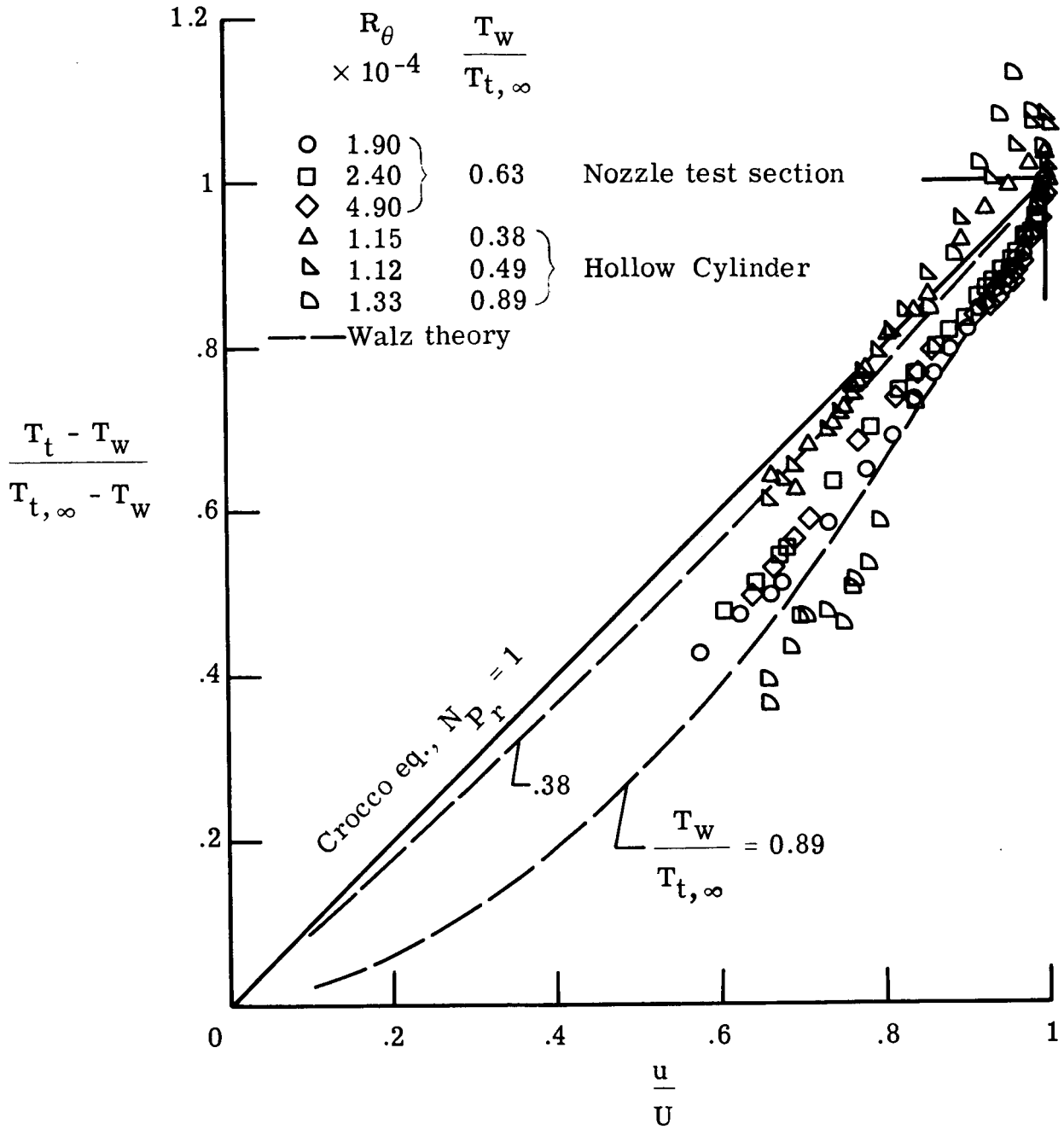

NASA

Figure 18.- Effect of wall temperature on the temperature-velocity profiles at $M_\infty = 6$ in the Langley 20-inch hypersonic wind tunnel.

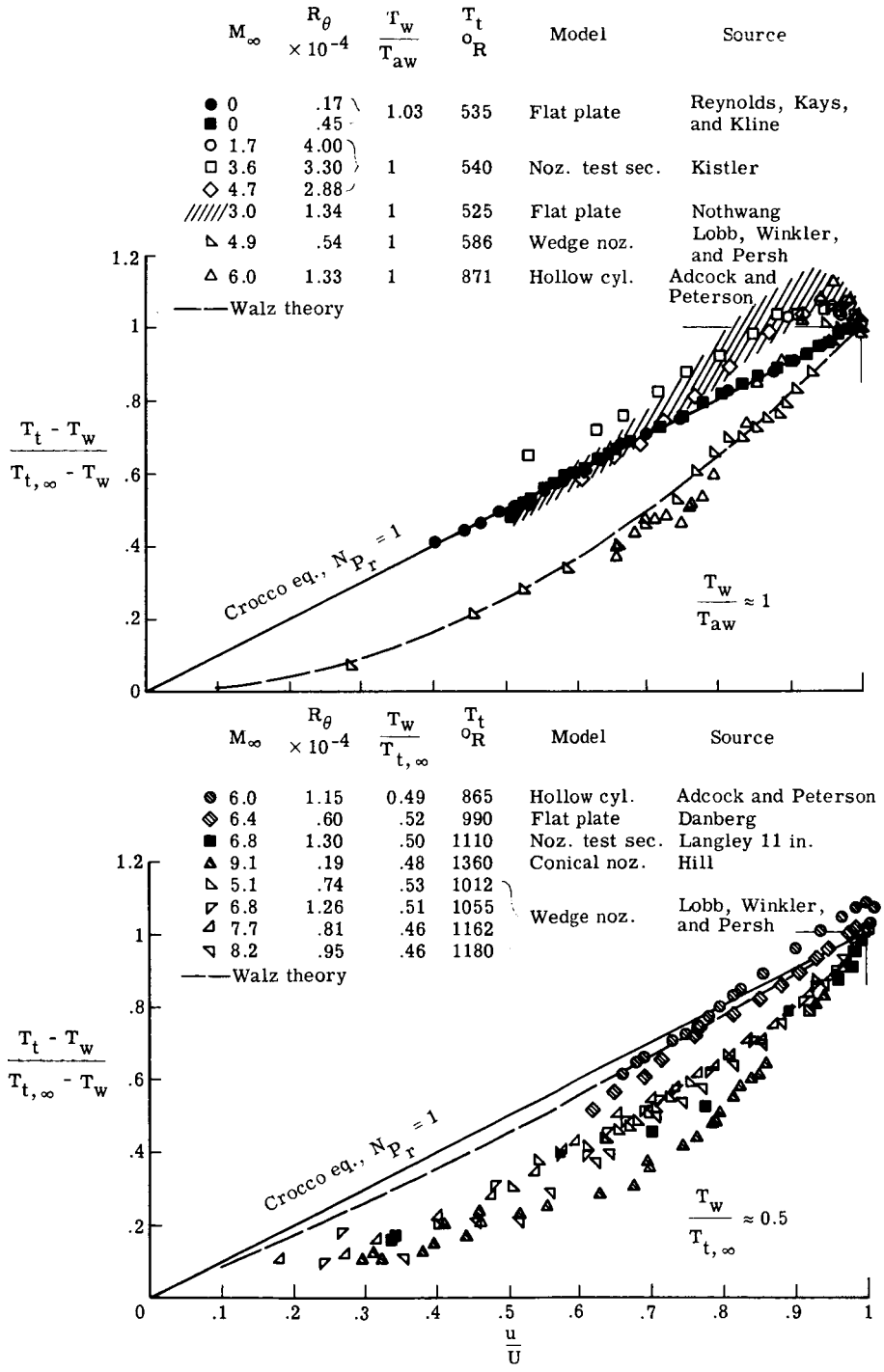

NASA

Figure 19.- Temperature-velocity profiles for two wall temperature ratios and various values of Mach number at the edge of the boundary layer.